Paleoceanography and Paleoclimatology

AGU ADVANCING EARTH AND SPACE SCIENCE

RESEARCH ARTICLE
10.1029/2022PA004566

**Key Points:**

- Laminae of the Upper Miocene diatomaceous Pisco Formation reveal that the fall dump mechanism regulated marine export production
- The predominance of fall dump over upwelling implies a drop of the temperature gradient between the Western and Eastern Pacific
- Evidences highlight a need of caution when using biogenic silica as a proxy for paleo upwelling

**Supporting Information:**

Supporting Information may be found in the online version of this article.

**Correspondence to:**

K. Gariboldi,
karen.gariboldi@unipi.it

**Citation:**

Gariboldi, K., Pike, J., Malinverno, E., Di Celma, C., Gioncada, A., & Bianucci, G. (2023). Paleoceanographic implications of diatom seasonal laminations in the upper Miocene Pisco Formation (Ica Desert, Peru) and their clues on the development of the Pisco Fossil-Lagerstätte. *Paleoceanography and Paleoclimatology*, *38*, e2022PA004566. https://doi.org/10.1029/2022PA004566

Received 10 OCT 2022
Accepted 20 APR 2023
Corrected 18 MAY 2023

This article was corrected on 18 MAY 2023. See the end of the full text for details.



# Paleoceanographic Implications of Diatom Seasonal Laminations in the Upper Miocene Pisco Formation (Ica Desert, Peru) and Their Clues on the Development of the Pisco Fossil-Lagerstätte

**Karen Gariboldi[1], Jennifer Pike[2], Elisa Malinverno[3], Claudio Di Celma[4], Anna Gioncada[1], and Giovanni Bianucci[1]**

[1]Dipartimento di Scienze della Terra, Università di Pisa, Pisa, Italia, [2]School of Earth and Environmental Sciences, Cardiff University, Cardiff, UK, [3]Dipartimento di Scienze dell'Ambiente e della Terra, Università di Milano-Bicocca, Milano, Italia, [4]Scuola di Scienze e Tecnologie, Università di Camerino, Camerino, Italia

**Abstract** The detailed study of diatom laminations conducted by means of backscattered electron imaging serves as tool to unravel details of past ocean dynamics. In this paper we apply this method to the analysis of the diatomites of Cerro Los Quesos, Upper Miocene Pisco Fm, Peru. Numerous studies have been conducted on the Pisco Fm; however, a focus on its paleoceanographic significance is still lacking. In this work, we provide information on the oceanographic setting in the area at the time of diatomites deposition. The high abundance of deep-living *Coscinodiscus* laminae, proceeded by either a mixed lamina or a terrigenous one, let us hypothesize a deep position of the thermocline during the deposition of the Pisco diatomites; together with the scarcity of *Chaetoceros Hyalochaete* spp. resting spores, this evidence confutes the belief that equals high biogenic silica content in marine sediments with enhanced upwelling. Conversely, the depositional setting of the Pisco Fm diatomites is more similar to what is known as "permanent El Niño" (or "El Padre") state, meaning a constant weakened upwelling (or upwelling of nutrients-poor waters). Climate modeling warns that an increase in atmospheric $CO_2$ may lead to this mean state in the near future. Thanks to this study we also obtained refined information on the diatomites sedimentations rates. The comparison of the Pisco diatomites sedimentation rates with those of Quaternary diatomites gave strength to the hypothesis that the formation of the vertebrate Lagerstätte may have been enhanced, among others, by the so-called "impact-burial" mechanism.

**Plain Language Summary** Some sedimentary rocks are formed by the remains of small organisms. This is the case of diatoms, microscopic algae with a siliceous exoskeleton. As we know the ecological conditions of the modern oceans in which different diatom species live, when we found them in sedimentary rocks, we can infer the ecological conditions of the oceans millions of years ago. Here, we present the species that we found in some Peruvian rocks, the so-called Pisco Formation, which dates back to 7/6 Million of years ago. Different species are preserved in these rocks in the same order in which they bloomed, so that we can identify small "laminae" (horizontal strips in the rock with thicknesses smaller than 1 mm) for each blooming season. The species that we recognize are those that today bloom during "El-Niño," a climatic warm condition that causes loss of large fishery stocks, inundations and droughts. This small finding helps us hypothesize how climate may evolve if the Earth's temperatures keep on rising. Also, the Pisco formation is famous because of their huge content of fossil whales and dolphins, thus the study of this rock helps us understand how these large mammals got preserved trough millions of years.

## 1. Introduction

The Late Miocene Pisco Fm, southwestern Peru, is an exceptional marine vertebrate Lagerstätte. Although its vertebrate fossil content has been deeply investigated for years (Bianucci, Di Celma, Collareta, et al., 2016; Bianucci, Di Celma, Landini, et al., 2016; Collareta et al., 2015, 2021; Esperante et al., 2015; Gioncada et al., 2016; Lambert et al., 2010; and references therein), an interpretation of the paleoceanographic setting existing during the Pisco Fm deposition is still lacking. This deficiency contrasts with the informative potential on the paleoceanography of the area that these sediments hold. Indeed, part of the formation, as observed at the site of at Cerro Los Quesos (CLQ, Pisco Fossil Lagerstätte Ica Desert, Peru; Figures 1a and 1b), is made up of laminated diatomites, of which existing literature has largely proved the potential.

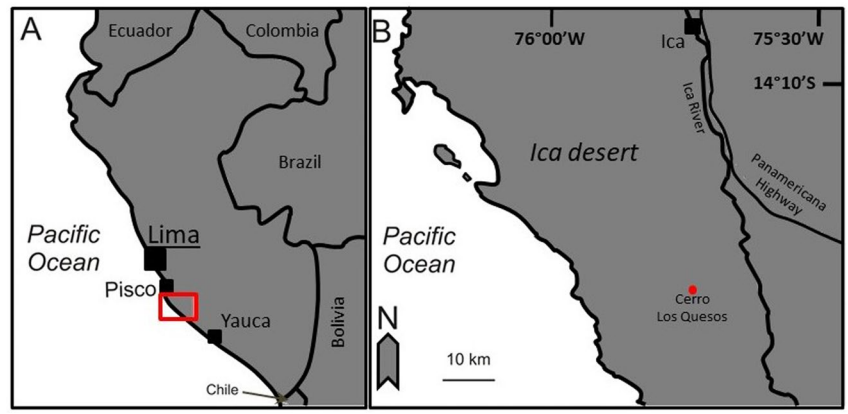


**Figure 1.** Geographic setting of the Ica desert. (a) Sketch map of Peru, with location of the Ica desert (red square). (b) Close up of the Ica desert; location of Cerro Los Quesos.

Previous high-resolution studies of laminated diatom-rich marine sediments have provided important insights into past seasonal cycles of phytoplankton productivity (Davies & Kemp, 2016; Davies et al., 2009; Kemp et al., 2000; Maddison et al., 2012; Pike & Stickley, 2013; Pike et al., 2001; Stickley et al., 2005) by comparing the sequences of laminations with modern diatom seasonal assemblages obtained from sediment traps (e.g., Dunbar & Berger, 1981; Sancetta, 1995; Thunell et al., 1993) in different environments, such as upwelling areas (Peruvian forearc basins: Brodie & Kemp, 1994, Kemp, 1990; Gulf of California: Pike & Kemp, 1996b, 1997, 1999; Santa Barbara Basin: Bull et al., 2000), enclosed seas, as the Mediterranean Sea (Corselli et al., 2002; Kemp et al., 1999) and Black Sea (Pilskaln & Pike, 2001), the Southern Ocean (Alley et al., 2018; Grigorov et al., 2002; Tesi et al., 2020).

In their study on Pleistocene laminae from the Santa Barbara Basin, Bull et al. (2000) were able to recognize evidence of El Niño events. These were reflected in the frequency of terrigenous laminae representing the continental runoff caused by the intensified rainfall associated to this phenomenon. In the coastal water of Peru, the modern El Niño Southern Oscillation (ENSO) causes a warming of the subsurface water and the consequent deepening of the thermocline (e.g., Caviedes, 1984). This condition modifies the regular Peruvian upwelling regime (the periodicity observed today is of ca. 3–7 years; Adamson, 2019), by preventing the south-easterly winds to act on the deep cold and nutrient-rich waters segregated under the deeper thermocline. As a consequence, primary production in surface waters declines, causing the loss of large fishery stocks (during 1997–1998 El Niño event, Peruvian fishery export dropped by 66%), inundations along the coast and droughts in the inlands (e.g., Caviedes, 1984).

El Niño Southern Oscillation-like variability has been observed in the laminated diatomites of the Upper Cretaceous Marca Shale, California (Davies et al., 2012). Marty (1988) suggests that Eocene laminated diatomites from Fundo Desbarrancado (Southern Peru) testifies an upwelling regime already taking place during the Eocene. Most recent studies based on reconstructing the Pacific surface temperature measuring the Mg/Ca ratio on foraminifera tests have highlighted the presence of the El Niño phenomenon during the Pliocene (Ravelo et al., 2006, 2014 and references therein; White and Ravelo 2020a, 2020b and references therein). These studies suggested us that the investigation of the Miocene diatomaceous laminae of the Pisco Fm may have helped us found the climatic mechanisms that regulated the seasonal stratification of the water column in the area.

As a second step, we have wanted to test the possibility of getting indications of the role played by the flux of diatoms to the sea bed in preserving the carcasses and thus leading to the formation of the Lagerstätte. We can get a glimpse of the importance of this Lagerstätte in terms of: (a) number of findings by citing the data reported by Bianucci, Di Celma, Collareta, et al. (2016), Bianucci, Di Celma, Landini, et al. (2016), where the authors list more than 300 specimens preserved as bone elements belonging mostly to cetaceans at the site of Cerro Colorado (Pisco Fossil Lagerstätte Ica Desert, Peru) and 192 fossils of marine vertebrates preserved as bone elements at CLQ; (b) the exceptional preservation of the specimens, both in terms of completeness and details of delicate features such as baleens (e.g., Bosio et al., 2021a; Collareta et al., 2021; Esperante et al., 2015), and; (c) the scientific relevance of this findings by recalling that the Miocene represents a pivotal moment in the evolution of marine vertebrates (Marx & Uhen, 2010).

Recently, researches have investigated the mechanisms that have favored the fossilization of all these organisms. Brand et al. (2004) and Esperante et al. (2008, 2015) were the first to hypothesize some of the mechanisms that may have led to the development of the Lagerstätte, citing early mineralization of the carcasses due to the rapid burial and sedimentation rates in the Pisco Fm two to four orders of magnitude higher than in modern analogs. The mechanism invoked to justify such a high sedimentation rate is a "strong ocean upwelling" (Esperante et al., 2015), which, according to the authors, is indicated by the abundance of the diatom species *Thalassionema nitzschiodes*. Yet, neither Esperante et al. (2008, 2015), nor Brand et al. (2004) present in their papers diatom species counts or age models.

Only some more recent papers (Bosio et al., 2021a, 2021b; Gioncada et al., 2016, 2018a, 2018b) explored in detail the cause of the rapid mineralization of the carcasses and the sedimentation rates in the Pisco Fm. In particular, Gariboldi et al. (2017) were able to calculate the sedimentation rate of a stratigraphic section measured at CLQ, this being equal to 19 ± 1 cm/ka. This estimate is high, but not exceptional if compared with sedimentation rates of other high productivity basins. However, we must underline that it was calculated using few tie points (either diatom bioevents or $^{40}Ar/^{39}Ar$ ages from volcanic ash layers). Considering this limit, we decided to expand our knowledge on the influence of diatom deposition on fossil preservation, by studying in detail the diatomaceous laminae characterizing part of the stratigraphic section at CLQ. Such approach provides estimates of the annual sedimentation rates in the basin during the deposition of diatomites, by recognizing the annual repetition of species blooms in the sediments: the thickness of annual sequences corresponds to the yearly sedimentation rates.

As such, although our information are limited to a small sample, in this paper we debate on the paleoclimatic significance of the CLQ laminae sequences and conclude presenting the implications that the sedimentation rates of the diatomaceous laminae had on the formation of the fossil Lagerstätte.

## 2. Materials and Methods

The Pisco Fm crops out along the southwestern coast of Peru, from Pisco to Yauca (ca. 300 km, Figure 1a), for about 300 km, with a thickness ranging from 200 to 1,000 m (Dunbar et al., 1990). It was deposited during the Mio-Pliocene, resulting as the youngest sedimentary unit filling the East Pisco forearc basin (De Muizon & DeVries, 1985; DeVries, 1988; Thornburg & Kulm, 1981), which started to uplift in the Pliocene, mostly due to the subduction of the aseismic Nazca ridge under the South American plate (Hsu, 1992). Nowadays, the East Pisco Basin belongs to the so-called "Pampas Costera" (Coastal Desert), a desert region cluttered with numerous hills with a large base and a planar top (Montoya et al., 1994) and with their stratigraphical top characterized by laminated diatomites (but also by nodular dolomite layers, terrigenous sandstones, tuff beds and phosporites: Brand et al., 2011; Dunbar et al., 1990; Di Celma et al., 2016; Malinverno et al., 2023). Cerro Los Quesos, CLQ, is one of these hills.

After numerous field campaigns undertaken between 2007 and 2015, a total of 192 fossil marine vertebrates were censed at CLQ in an area of approximately 4 $km^2$ (Bianucci, Di Celma, Lambert, et al., 2016). Information, such as the specimens' position, taxonomy, degree of completeness, degree of articulation and potential presence of dolomite nodule enclosing the bones were collected on dedicated sheets (Gariboldi et al., 2015).

The stratigraphic position of the fossils was based on the geological investigation and mapping carried out at CLQ by Di Celma et al. (2016). These authors subdivided the sedimentary succession exposed at CLQ in 6 informal lithological members that were labeled from A to F in stratigraphic order. The vertebrate census allowed to point out that 92.7% of the fossils are preserved in the "F member," which is composed mainly of a monotonous succession of finely laminated white diatomites (Di Celma et al., 2016). Considering that, due to the paucity of tie points, specific sedimentation rates were not calculated for each informal member (Gariboldi et al., 2017), in this study we try to identify seasonal laminae cycles in the F member to calculate the yearly accumulation rates of sediments into the basin during its deposition.

Using a metal conduit, a 25-cm-thick sample of laminated diatomaceous mudstone was collected in the F member of the CLQ stratigraphic succession, from under a vertebra of a fossil whale (Figure 2a) called CLQ M58 (Figure 2; hereafter M58. Specimen position: 14°30'58.3"S; 75°43'04.5"W; 167.0 m above the base of the measured section (abs), Bianucci, Di Celma, Lambert, et al., 2016).

The conduit was placed on the outcrop surface and sediments were excavated around the conduit profile. In this way, the conduit slid into the outcrop encapsulating the intact sediment section. Next, the protected sample was

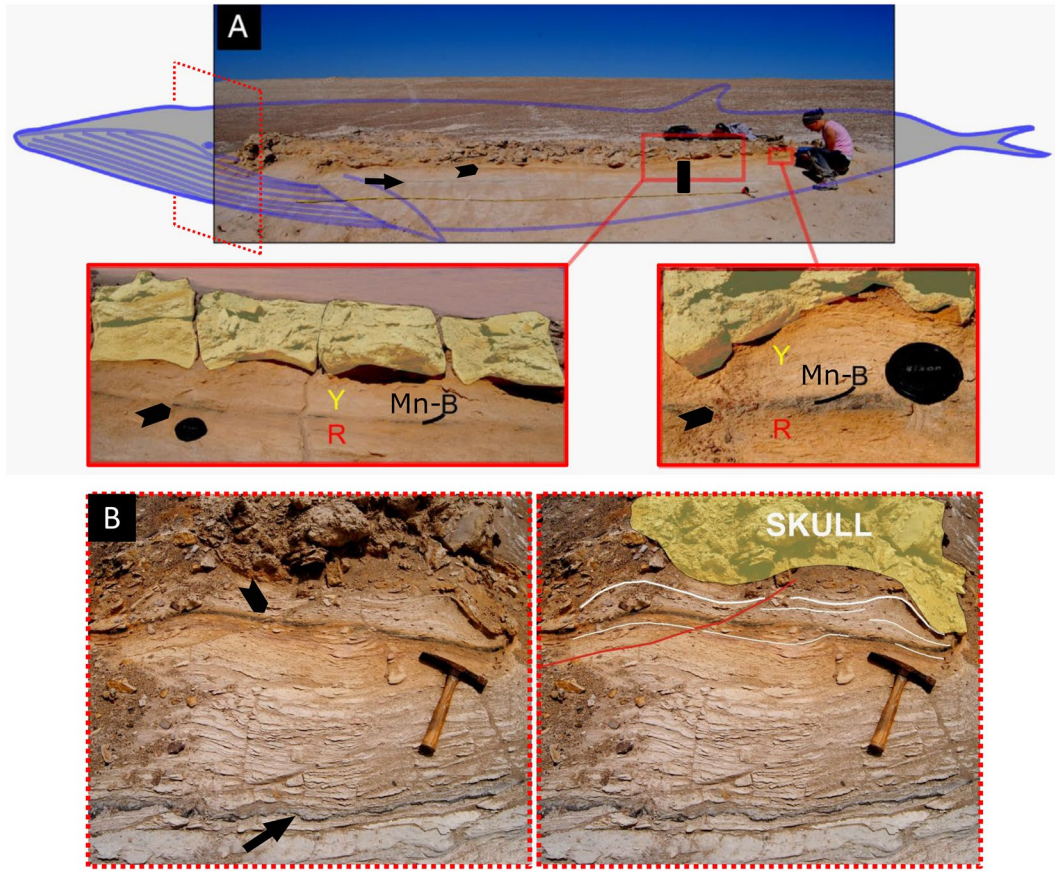


**Figure 2.** Fossil whale Cerro Los Quesos (CLQ) M58 (14°30′58.3″S; 75°43′04.5″W) at Cerro Los Quesos, Ica Desert, Peru. (a) CLQ M58 in the outcrop. Black rectangle: location of the CLQ20 sample; black arrow: black tephra underneath CLQ M58 (not dated); black arrowhead: Mn layer of the YBR sequence (see text for explanation). The two red rectangles show the yellow portion of diatomites ("Y") underlain by a black manganese-rich layer ("Mn-B") and by reddish diatomites ("R") related to geochemical processes activated by the decomposition of the carcass (see Gariboldi et al., 2015; Gioncada et al., 2018a, 2018b). Camera dust cap for scale. The red dotted square highlights the position of (2b) in respect to M58. (2b). Detailed of the diatomites below the skull of M58; right: the sedimentary features observed in the left picture are outlined. Laminations (white lines) are deformed by the weight of the skull (yellow area) and in some points cut by the Mn layer (black arrowhead in the left picture). These deformations highlight that the carcass sank into the soupy, plastic diatomitic sediments as it reached the seabed. The geometry of the Mn layer with respect to the laminations shows that it precipitated after the diatomites were deformed. Red continuous line highlights secondary deformations. The black arrow points to the black tephra layer. Hammer as a scale. Modified from Bosio et al. (2021a) and Gariboldi et al. (2015).

dug out of the outcrop. This technique facilitated the preservation of the 25-cm sequence and its stratigraphy. The sample was named CLQ20 (Figure S1 in Supporting Information S1). Besides the fact that M58 is located in the F member, we decided to collect the sample for laminae analysis under it because: (a) M58 represents an almost complete and still articulated specimen, therefore representing a good example of exceptional preservation of the Pisco Lagerstätte; (b) the sediments directly underlying M58 are not only laminated, but also characterized by a typical sediment geochemical perturbation (the yellow-black-red sequence described by Gariboldi et al., 2015 and Gioncada et al., 2018a in the frame of the taphonomic studies of the Pisco Lagerstätte; see details of Figure 2a) derived by diagenetic processes that bring to the precipitation of a dolomite nodule around the whale carcasses, therefore allowing us to have a complete frame of the different taphonomic processes that a carcass can undergo; (c) M58 is located on the top of the CLQ hill, on a morphological plateau that facilitates the access to the specimen, its observation and the sampling of the underlying sediments; (d) stratigraphically, M58 is placed between two dated volcanic ash layers: the older, the so called "Mono" ash layer, has an age of 6.93 ± 0.09 Ma, while the younger has a lower limit of ≥6.71 ± 0.02 Ma (Di Celma et al., 2016; See Text S1 in Supporting Information S1), therefore dating M58 and the CLQ20 sample back to the Messinian (Figure 3). The age of these rhyolitic ashes was provided by $^{40}Ar/^{39}Ar$ dating of biotite (Di Celma et al., 2016).

Small, 4–5 cm subsamples of CLQ20 oriented perpendicular to the lamina fabric were embedded in epoxy resin (Araldite 2020) using a vacuum chamber and a total of 15 (Figure S1 in Supporting Information S1) polished thin sections were prepared for scanning electron microscope backscattered electron imagery (BSEI) analysis (Kemp, 1990; Pike & Kemp, 1996a). Thin sections were carbon-coated and analyzed in backscatter mode using a Veeco FEI -Philips- XL30 environmental scanning electron microscope in the School of Earth and Environmental Sciences, Cardiff University and a Hitachi TM 3030 SEM at the Department of Earth Sciences, Pisa University. One thousand two hundred and eighty-four BSEI images were taken to construct 20 BSEI photomosaics at 100x, 800x, and 2000x magnification; and more than 400 high magnification images were collected. Only some selected images are presented in this work.

Laminations were described using four parameters: relative bimodality, laminae content (terrigenous or biogenic particles, diatom species composing each lamina), laminae boundaries (straight or wavy, sharp or blunt) and laminae lateral continuity.

The relative bimodality is, as described by Grimm et al. (1996), the relative difference in gray value between adjacent laminae. However, differing from Grimm et al. (1996), we evaluated the bimodality from the BSE images and not from X-radiograph. The difference in gray value on a BSE image depends on the atomic number of the element hit by the electron beam. Terrigenous particles have a higher atomic number than the epoxy resin filling the pores of diatoms and therefore appear lighter. As such, as stated by Grimm et al. (1996), high bimodality (HB) couplets are more evident where pure diatomaceous ooze laminae juxtapose terrigenous laminae. Conversely, low bimodality couplets (LB) are made of discernible laminae but with a very low gray contrast (as in the case of two diatomaceous laminae bearing different species associations). An intermediate situation between HB and LB is defined as moderate bimodality (MB).

## 3. Results

### 3.1. The CLQ M58 Whale and the CLQ20 Sample: In Situ and Macroscopic Observations

The M58 whale is an indertermined Balenopteroidea censed by Bianucci, Di Celma, Landini, et al. (2016) in the F member of the sedimentary succession exposed at CLQ and described as an articulated skeleton with the skull eroded (Table 1 of Gariboldi et al., 2015 and Figures 2a and 2b of this work). M58 lies on a yellow portion of diatomites underlain by a black manganese-rich layer and reddish diatomites (Figures 2a and 2b, black arrowhead) related to geochemical processes activated by the decomposition of the carcass (see Gariboldi et al., 2015; Gioncada et al., 2018a; see in particular paragraph 3.5 and Figure 5 of Gioncada et al., 2018a for explanations). Therefore, we consider the Mn layer as the boundary between sediments influenced by the presence of the carcass (sediments above the Mn layer) and those not influenced by its presence (sediments below the Mn layer). Below the reddish layer the diatomaceous mudstone shows millimetric white-to-dark gray laminations. The CLQ20 sample represents the sediment under M58 from the yellow diatomites to the gray laminated diatomaceous mudstones, which are interrupted near the bottom of the sample by a 5 mm-thick black tephra (Figures 2a and 2b, black arrow); unfortunately, the latter could not be dated because of the lack of both biotite and sanidine crystals.

Detailed field observation of the skull of M58 highlighted that the lamination was deformed and in some points cut by the Mn layer (Figure 2b). This deformation strongly resembles the shape of the side of the skull lying on the diatomites and, as suggested by Bosio et al. (2021a), could be the evidence of the sinking of the carcass into the soupy but plastic diatomitic sediments as it reached the seabed.

### 3.2. Sediment Bimodality, Laminae Content, Styles, Sequences, and Laminae Thicknesses

Visual analysis of the low magnification mosaics (100x) was used to give a general evaluation of the bimodality pattern of the sediment. The sediment appears to be mainly characterized by low to moderate or MB (L-MB or MB; Figure 4a, 5a, 6a, 7a), which is mostly given by the sparse presence of silt particles. Silt particles appear very light in BSE images, within a dominant dark matrix made of the siliceous diatom frustules (Figures 4c, 4d, 4g, 4j, 5c, 5d, 5e, 5f, 5h, 5j, 5l, 5m, 7d, 7e, 7f, 8g, and 8h). Only rarely the bimodality is high (HB) and this condition is always verified where the terrigenous components dominated by clay particles are grouped to form laminae overlying and overlaid by biogenic ones (Figures 6a, 7a, and 8a).

On the basis of the laminae content we can identify.

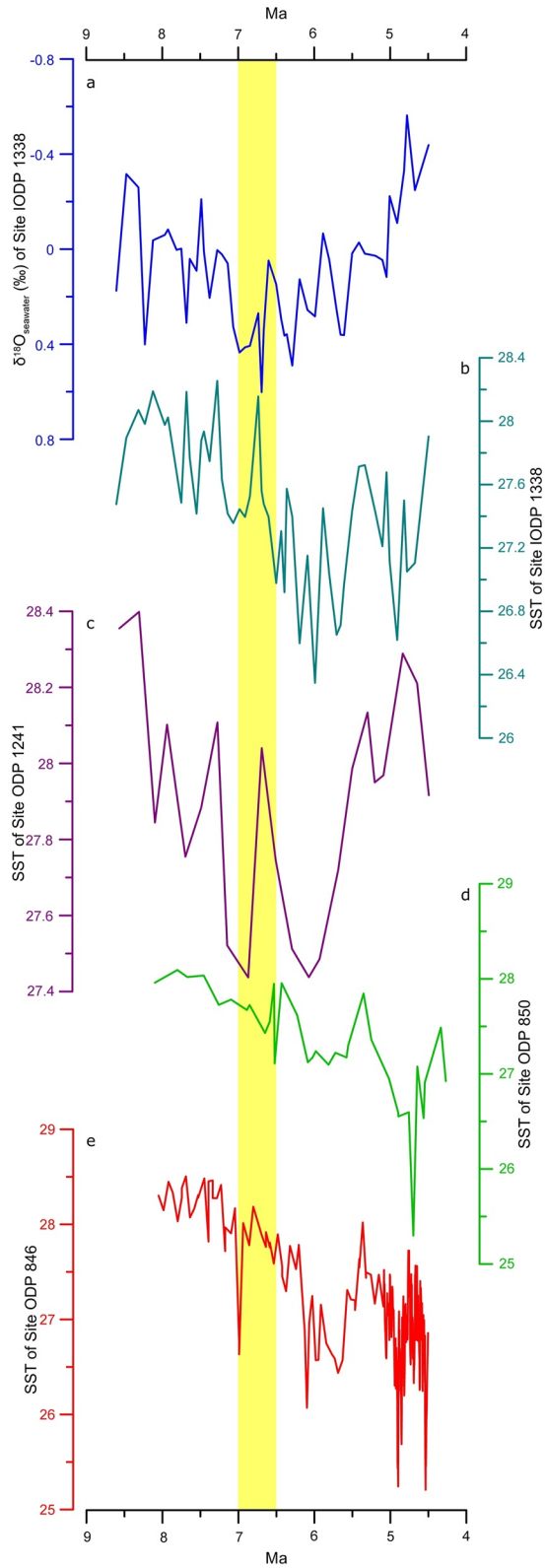


**Figure 3.**

1. Terrigenous laminae: laminae where terrigenous particles are >90% of the laminae. In CLQ20 these laminae are mostly made by clay particles (Figures 6b, 6e, 7b, 7c, 7f, 8d, 8e, and 8f), but also some silt particles (Figures 8a and 8d) or biogenic particles, such as rare *Thalassionema* specimens (Figure 6c), or other species (Figure 8d).
2. *Coscinodiscus* laminae: in this paper we use the definition "*Coscinosdiscus* lamina" to indicate a diatomite (a hard pelagic sediment made by >30% of skeletal remains of diatoms and <30% silt and clay, as defined by Palmer et al., 1986) where *Coscinodiscus* (possibly *Coscinodiscus asteromphalus;* Table 1) is the dominant genus (>90%; Figures 4b, 4e, 5b, 5f, 5g, 5i, 5k, 5m, 8a, 8c, and 8g). Other rare components of these laminae are *Actinocyclus octonarius* (Table 1) specimens (Figure 4f), *Thalassionema* specimens (Figure 8b; Table 1) and rare terrigenous particles (Figure 4e).
3. Mixed laminae (Figures 4a, 4b, 4g, 4h, 4i, 4j, 5a, 5b, 5c, 5d, 5e, 5h, 5j, 5l, 6a, 6b, 7a, 7d, 7e, 7f, 8a, and 8h): these are laminae composed of clay and silt particles in different percentages (Figures 4b, 4c, 4d, 4g, 4i, 5b, 5c, 5d, 5e, 5h, 5l, 5j, 7d, 7e, 7f, 8a, and 8h), specimens of *Coscinodiscus* (Figures 4b and 4j; sometimes the presence of *Coscinodiscus* in mixed laminae is due to an interdigitation of *Coscinosidiscus* laminae with mixed laminae as in Figure 5l) *Actinoptychus* (Figures 4h, 5d, red circle, probably *Actinoptychus senarius*; Table 1), *Stephanopyxis* (most probably *Stephanopyxis turris*, Figures 4g, 4j, and 5e, red circle; Table 1) and *Chaetoceros Hyalochaete* spp. resting spores (CRS; Figures 4i and 8h; Table 1). The percentages of these different components vary in each mixed lamina.
4. *Actinoptychus* cf. *senarius* laminae: rare diatomites where *Actinoptychus* cf. *senarius* represents >90% of the diatom species (Figures 6a, 6d, and 6e; Table 1).

Straight lamina boundaries in sample CLQ20 are rarely found and difficult to be traced, as the transitions from one lamina to the next are often indistinct. More frequently, boundaries are wavy (Figures 4b, 5b, and 6d) and, as said, indistinct, especially when representing the limit between a diatomaceous lamina and a mixed lamina (Figures 4a and 4b). Only in slide t14 quite distinct boundaries between a *Coscinodiscus* lamina and the over- and underlying mixed laminae are recognizable at low magnification (Figure 5a, dotted lines). Noteworthy, the only sharp boundaries are those delimiting terrigenous clayey laminae from others (Figures 6a, 6b, 7a and 8a). Boundaries between these laminae and the others are normally less wavy (then those between biogenic laminae) or straight (Figure 6a—white arrows; Figures 7a, 8a); also clots of clay can be observed throughout some slides, resembling a terrigenous lamina, but having a boudinage-like aspect (Figure 6a—arrowheads; Figure 7a—arrowheads and arrows on the right side of the figure). We do not consider them laminae as they are very thin (also <<100 μm). These clots have very straight and distinct boundaries, just as terrigenous laminae (Figures 7b and 7f) (see Table 1)

Both composition and boundaries of laminae help in verifying if they are laterally continuous; in CLQ20, although boundaries are normally indistinct, they are typically continuous (Figures 4a, 5a, 6a, 7a and 8a) and discontinuous laminae are present.

A deeper investigation at 800 and 2000x magnification helped the identification of different sequences of laminae, in particular.

1. The mixed lamina-*Coscinodiscus* lamina duplet (Figures 4b, 5b; Figure S2 in Supporting Information S1)
2. The terrigenous lamina-*Coscinodiscus* lamina duplet (Figure 8a);
3. The mixed lamina-*Actinoptychus* cf. *senarius* lamina duplet (Figures 6a, 6d, and 6e).

The last case was observed only once and, therefore, it is considered rare. Also the terrigenous lamina-*Coscinodiscus* lamina duplet is evident only in one case (Figure 8a). In Figure 7a some clots of clay topping the mixed laminae can be observed (arrows on the right of the photo); these have a frequency of 3–3.5 mm, made exception for the first one, which is ca. 1 mm apart from the underlying terrigenous lamina. Similar clots overlying a mixed lamina are observed in slide t5 (Figure 6a—arrowheads, Figure 6e).

Comparing at higher magnification (Figure S2 in Supporting Information S1) the t9 slide (Figure 7a) for its whole length it appears clearly that the sediment is mainly composed of the mixed lamina-*Coscinodiscus* lamina duplet,

**Figure 3.** Temporal context of the CLQ20 sample and $\delta^{18}O$ and SST values for the Eastern Equatorial Pacific in the 9–4 Ma range. Sample CLQ20 was deposited between an older age limit of 6.93 ± 0.09 Ma, and a younger lower limit of ≥6.71 ± 0.02 Ma (yellow rectangle; Messinian), as suggested by two dated tephra in the Cerro Los Quesos stratigraphic succession; (a) the $\delta^{18}O_{seawater}$ (‰) for IODP Site 1338 (Rousselle et al., 2013) and SST (°C) values for: (b) IODP Site 1338 (Rousselle et al., 2013); (c) ODP Site 1241 (Seki et al., 2012); (d) ODP Site 850 (Zhang et al., 2014a, 2014b); (e) ODP Site 846 (Liu & Herbert, 2004). The CLQ20 sample dates back to a period characterized by high values of $\delta^{18}O_{seawater}$ and SST as high as during the Middle Pliocene Warm Period (see Figure 5 of Rousselle et al., 2013). All SST shown are calculated following the $U^{k'}_{37}$ calibration proposed by Müller et al. (1998).

10.1029/2022PA004566

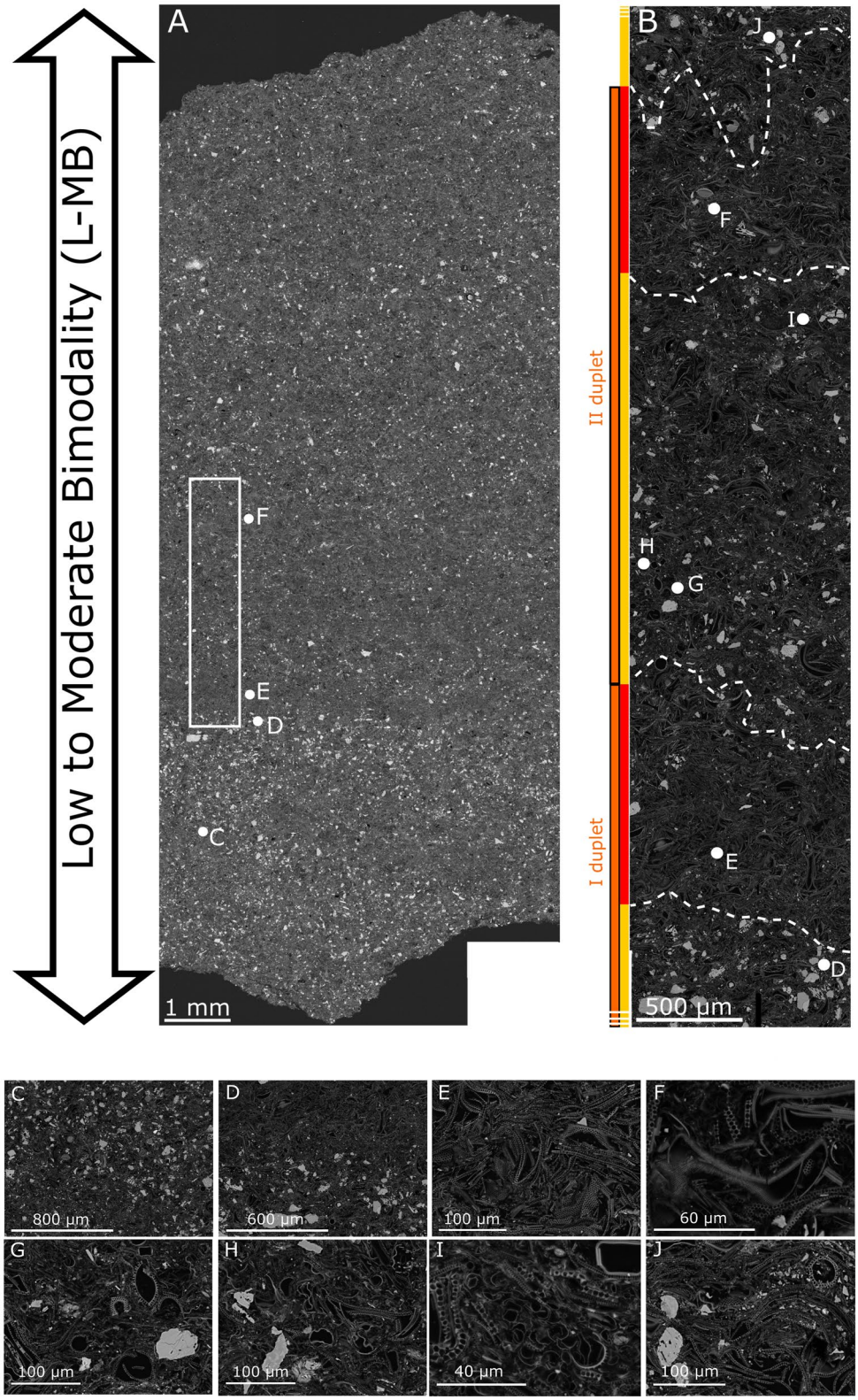


**Figure 4.**

the mixed laminae being topped by clay clots (Figure 7a—arrows; Figure S2 in Supporting Information S1—arrows). As the t9 slide is defined by a MB (Figure 7a) we consequently translated the MB and L-MB feature (Figures 4a, 5a and 7a) into sediment composition: in other words, we started considering the MB and L-MB equivalent to the presence of mixed lamina-*Coscinodiscus* lamina duplet. This deduction is confirmed by the investigations at higher magnifications of slides t13, t14, t9 images (800 and 2000x: Figures 4b, 5b, 8a), where this duplet prevails. As the L-MB and MB are the mostly observed throughout the CLQ20 sample, we deduce that the mixed lamina-*Coscinodiscus* lamina duplet is the one most frequent in CLQ20.

The mixed lamina-*Coscinodiscus* lamina duplet shows very different thicknesses, the three highlighted in Figure 5b varying from ca. 625 µm to ca. 1,750 µm, with a huge difference in the thickness of the two mixed laminae (ca. 375 µm in the second duplet vs. ca. 1,500 µm in the third duplet). Differences in the thickness of *Coscinodiscus* laminae are nonetheless noteworthy: on one hand, the *Coscinodiscus* lamina of the second and third duplets are similar (varying from ca. 250–500 µm); on the other hand the *Coscinodiscus* lamina of the first (highlighted with an asterisk) and second duplets are ca. 1,000 µm thick (Figure 5b). The lower boundary of the mixed lamina of the first duplet is not clear, therefore we do not report the thickness of the whole duplet. Significantly, also in the duplet terrigenous lamina-*Coscinodiscus* lamina observed in Figure 8a, the latter is ca. 250 µm as in the two cases in Figure 5b; its terrigenous companion is ca. 650 µm thick (Figure 8a), the thickness of the whole duplet being ca. 900 µm.

## 4. Discussion

### 4.1. Paleoclimatic Implications of the Pisco Fm. Diatom Laminae

There are at least three features confirming that laminae in the CLQ20 sample are the product of a primary deposition process: (a) the recurrent patterns of laminae in the CLQ20 sediments, in particular the mixed lamina-*Coscinodiscus* lamina; (b) the very well-defined boundaries of the terrigenous laminae; and (c) the lateral continuity of laminae.

The characteristic of the primary production inputs and of the terrigenous ones, can therefore be used as proxy for a paleoclimatic reconstruction of the area.

The studies of laminated sediments from the Peru forearc basins (Brodie & Kemp, 1994; Kemp, 1990) described upper Quaternary laminated sediments from the Peru shelf and upper slope. These were collected during ODP Exp 112 (Sites 680, 681, and 686) and during the R.R.S. Darwin Leg 38 (Sites 38.10 and 38.9). These studies highlighted the presence of three different groups of laminae; isolated, irregularly spaced and continuous sub-millimeter laminae. In all those three cases diatomaceous laminae are often mainly monospecific and composed of upwelling genera, such as *Skeletonema* and *Chaetoceros*. Conversely, *Coscinodiscus* oozes are rare. On the other hand, terrigenous laminae are either silt-rich (main thickness 600 µm, with a standard deviation of 350 µm) or clay-rich laminae (main thickness 550 µm, with a standard deviation of 500 µm), with the silt component not invariably present in the sequence (Brodie & Kemp, 1994). These laminae form a sub-millimeter couplet that is irregularly inter-laminated with diatom ooze. The oozes are controlled by the intensity of upwelling and/or the nutrient content of upwelled waters, while terrigenous laminae are the expression of regular rainfalls caused by the permanent presence of warm water off Peru during Isotope Stage 5 (Brodie & Kemp, 1994). The absence of diatom oozes between the silt/clay couplets is interpreted by the authors either as the result of absence of an algal bloom or the complete dissolution of the crop in the water column; both these hypotheses would suggest a reduction of nutrient availability, a feature which is consistent with El-Niño events (Brodie & Kemp, 1994).

*Coscinodiscus* spp. were associated with the "Fall dump" events, described for the first time in the Gulf of California, during the Holocene, by Kemp et al. (2000). The authors identify *Coscinodiscus* spp. specimens as

**Figure 4.** BSE-SEM images of slide t13. (a) Low magnification (100x) BSE image of slide t13, which is characterized by a low to moderate bimodality (L-MB). This bimodality pattern is mostly given by the sparse presence of silt particles within a darker matrix (diatomite). The white rectangle indicates the position of (b); letters highlight the same spots in panels (a and b) as well as in panels (c–j). The mixed lamina (yellow rectangles)—*Coscinodiscus lamina* (red rectangles) duplets (orange rectangles) are discernible. Mixed laminae are particularly recognizable due to the presence of silt particles. Boundaries between laminae (white dotted lines) are wavy and indistinct. Colored rectangles are dotted when laminae are not pictured in their whole length. (c) Silt particles in mixed lamina. (d) Boundary between a mixed lamina (bottom) and a *Coscinodiscus* lamina (top). (e). Detail of *Coscinodiscus* frustules in a *Coscinodiscus* lamina. (f) Detail of *Actinocyclus octonarius* frustules in a *Coscinodiscus* lamina. (g) Detailed of a mixed lamina; silt particles, *Stephanopyxis* frustules and *Actinoptychus* cf. *senarius* frustules are visible. (h) Detailed of *Actinoptychus* cf. *senarius* frustules in a mixed lamina. (i) A bunch of *Chaetoceros Hyalochaete* resting spores in a mixed lamina. (j) Detail of a mixed lamina: silt particles, *Coscinodiscus* frustules and *Stephanopyxis* frustules are visible.

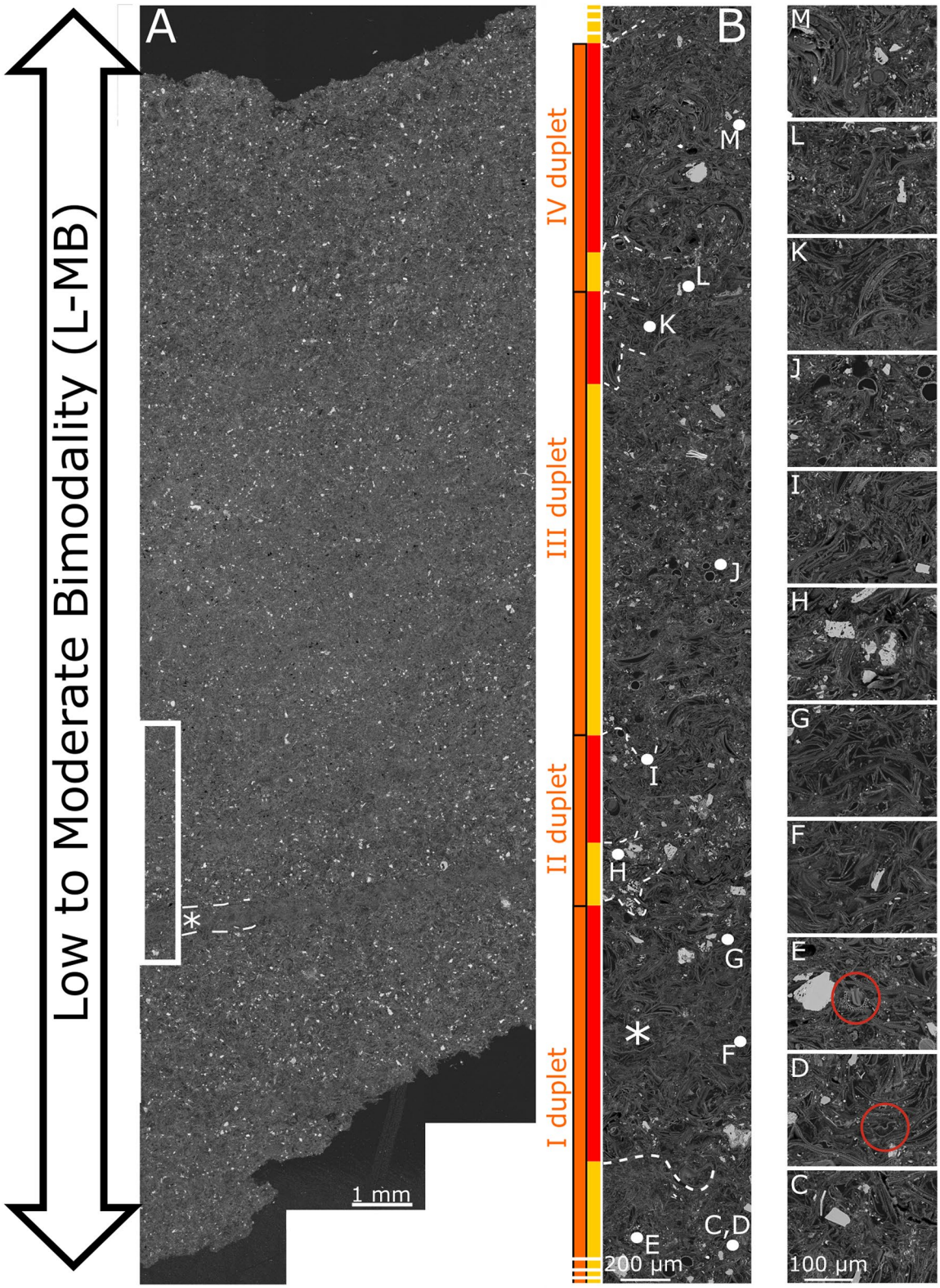


**Figure 5.**

"clusters of individuals rather than as contiguous sub-laminae" deposited above the diatomaceous laminae (made either of *Rhizosolenia* spp. or *Stephanopyxis palmeriana*) overlying the summer terrigenous lamina. Therefore, the authors include this genus among those that are able to thrive at the thermo/nutricline at low light conditions preferring a stratified water column, the so-called "shade" flora (Kemp et al., 2000; Sournia, 1982). Blooms of the "shade flora" may last throughout the periods of water stratification; the diatoms growing during this period start settling with the onset of fall/winter mixing (the "fall dump") (Kemp et al., 2000). These characteristics make them differ from the small subgenus *Chaetoceros Hyalochaete*, which thrives during upwelling conditions (spring) (Kemp et al., 2000). Somehow similarly, Romero and Hebbeln (2003), studying diatom assemblages of surface sediments below the Peru-Chile Current, list *Chaetoceros* species in the coastal upwelling group (together with *Thalassionema nitzschioides* var. *nitzschioides*), while they classify *Coscinodiscus argus* and *C. radiatus* in the coastal planktonic group (characterised by the presence of non-upwelling associated species). Yet, the authors find *C. argus* and *C. radiatus* together with *Chaetoceros* spp. between 34° and 38°S, highlighting that at those latitudes the primary production is due to both upwelling and proliferation of the fall dump flora during periods of water column stratification.

With these pieces of information, some interpretations can be given to the *Coscinodiscus* laminae, while no present analogue has been observed for the *Actinoptychus* cf. *senarius* lamina (Figures 6a, 6d, and 6e).

Indeed, the huge contribution of *Coscinodiscus* spp. to the diatom fraction in laminae of sample CLQ20 and the scarce presence of *Chaetoceros Hyalochaete* spp., which was observed only in small sparse clusters (Figures 4i and 8h), testify that primary production during the deposition of the F member was regulated by the stratification of the water column rather than by coastal upwelling; however, the presence of both phenomena in the same region, during different time of the year, is also plausible.

On one hand, the absence of *Rhizosolenia* spp. and *Stephanopyxis palmeriana* in the fall dump lamina suggests that the dominance of *Coscinodiscus* is not only related to stratification of the water column but also to some other ecological limiting factor. As *Stephanopyxis palmeriana* is known as a warm water (Drebes, 1966) tropical species (Molina et al., 1997), warmer than *Stephanopyxis turris* (Cupp, 1943), a species sporadically present in the CLQ20 sediments (Figures 4b, 4g, 4j, 5b, 5e, and 5j), it appears that water temperature may play a role in the absence of *S. palmeriana*. More generally, it can easily be assumed that the waters present in the Eastern Equatorial Pacific (EEP) Ocean during the late Miocene had different properties and origin in respect of those present in the Gulf of California during the Holocene; as such, it is not surprising that the dominant genera thriving at the thermocline in these two scenarios are different. Also Shankle et al., 2021 tested the possibility that water properties reaching the equatorial Pacific in the Late Miocene/Early Pliocene were different from today's (older, more acid and more nutrient-rich).

On the other hand, the absence of strong upwelling-related-*Chaetoceros* blooms, such as recorded in the laminae of the CLQ20 sample, may reflect a deepening of the thermocline in the EEP during the Messinian. Currently, this condition is registered during El Niño events: during the 1982–1983 El Niño, the winds were constantly upwelling-favourable but the thermocline was deeper than normal. Thus, as the source depth of upwelled water was the same of normal conditions (i.e., 50–100 m), upwelled waters were warm and poor of nutrients, as they came shallower than the thermocline (Huyer et al., 1987). Such a functioning of the El Niño was later confirmed by other authors (Hill et al., 1998; Strub et al., 1998).

With these observations in mind, when looking at the CLQ20 mosaics one may be tempted to say that the mixed lamina-*Coscinodiscus* lamina duplets, together with the terrigenous lamina—*Coscinodiscus* lamina duplets are

**Figure 5.** BSE-SEM images of slide t14. (a) Low magnification (100x) BSE image of slide t14, which is characterized by a low to moderate bimodality (L-MB). This bimodality pattern is mostly given by the sparse presence of silt particles within a darker matrix (diatomites). The white rectangle indicates the position of (b), while the asterisk highlights the position of a *Coscinodiscus* lamina particularly evident even at low magnification (this lamina is visible also in panels (b and f); dotted lines outlines part of the *Coscinodiscus* lamina boundaries, which are wavy, quite distinct and continuous. (b) 800x magnification of slide t14; four mixed lamina (yellow rectangles)—*Coscinodiscus* lamina (red rectangles) duplets (orange rectangles) are discernible, but the lowest one lacks the bottom of the mixed lamina. The sequence represented in panel (b) ends with the bottom of a mixed lamina (yellow rectangle). Colored rectangles are dotted when laminae are not pictured in their whole length. The mixed lamina—*Coscinodiscus* lamina duplets have thickness varying form 625 μm to ca. 1,750 μm, with a huge difference in the thickness of the two mixed laminae (ca. 375 μm in the second duplet vs. ca. 1,500 μm in the third duplet). The *Coscinodiscus* lamina of the second and third duplets have more similar thicknesses (ca. 250 μm) but the *Coscinodiscus* lamina of the first and fourth duplets are ca. 1,000 μm thick (thickness of laminae are approximate as their thickness vary along their length). Letters highlights the position of images in the right column. (c) silt particles in a mixed lamina. (d) *Actinoptyhcus* cf. *senarius* frustule in a mixed lamina (circled in red). (e) Silt particle and *Stephanopyxis* valve (circled in red) in a mixed lamina. (f, g) *Coscinodiscus* frustules and silt particle in a *Coscinodiscus* lamina. (h) Silt particles and *Coscinodiscus* frustules in a mixed lamina. (i) *Coscinodiscus* lamina at its upper boundary with a mixed lamina. (j) *Stephanopyxis* frustules and silt particles in a mixed lamina. (k) *Coscinodiscus* frustules in a *Coscinodiscus* lamina. (l) Silt particles and *Coscinodiscus* frustules in a mixed lamina. (m) *Coscinodiscus* frustules and silt particle in a *Coscinodiscus* lamina. The 100 μm scale bar is valid for (c–m).

10.1029/2022PA004566




**Figure 6.** BSE-SEM images of slide t5. (a) Low magnification (100x) BSE image of slide t5, characterized at its bottom by a high bimodality, given by the contrast of a terrigenous lamina and the terrigenous boudinage-like top of a mixed lamina (arrowheads) with the underlying and overlying biogenic laminae. The rest of the slide is characterized by a low to moderate bimodality (L-MB). This bimodality pattern is mostly given by the sparse presence of silt particles within a darker matrix (diatomite). White arrows at the bottom point to the lower boundary of the terrigenous lamina, which is straight to wavy but sharp. The dotted line at the top of the image highlights a wavy boundary between a terrigenous lamina and the overlying *Actinoptychus* cf. *senarius* lamina. Letters highlights the position of images in the left column. (b) Detail of the lower boundary of the terrigenous lamina (the content of the underlying lamina is not defined, due to the imperfect polishing of the slide). (c) *Thalassionema* specimens in the terrigenous lamina. (d, e) Details of the boundary between the terrigenous lamina and the overlying *Actinoptychus* cf. *senarius* lamina; the white arrow in (d) points to an enlarged image of the *Actinophychus* cf. *senarius* frustules.

not only the expression of a El-Niño like condition, but, indeed of the El Niño condition itself (or, at least, of a proto El-Niño condition). Not only the paucity of CRS, together with the abundance of *Coscinodiscus* ssp., highlights a stratified water column with warm and nutrient-poor upwelled water: also the presence of silt particles in mixed laminae point to a rainy condition, which appears to increase its intensity periodically (as described by Bull et al. (2000), for late Quaternary in the Santa Barbara Basin and as it is known to happen today during El Niño phenomena; see for examples Caviedes, 1984; Hebbeln et al., 2000; Romero et al., 2002; Shipe et al., 2002) leading to the formation of clots of clay (Figure 7a—arrows; Figure S2 in Supporting Information S1—arrows). Briceño-Zuluaga et al. (2016) gave to the enhanced particle flux observed in the Pisco Basin during the Little Ice Age a similar interpretation.

Although aware that such affirmation is far too reckless (more data would be needed for such a statement), we still think that this observation may encourage to start to look better into diatomaceous records that may help us comprehend when and how the ENSO phenomenon started.

At present the El Niño phenomenon has been identified back to the Cretaceous (Davies et al., 2012) and to the so called "Middle Pliocene Warm Period," ca. 4.5–3.0 Ma (Fedorov et al., 2006; Ravelo et al., 2006; Ragaini et al., 2008; Wara et al., 2005; White & Ravelo, 2020a, 2020b. See Text S2 in Supporting Information S1). Some authors stated that, during the Middle Pliocene Warm Period the El Niño conditions was permanent, rather than showing a periodicity similar to that of recent days: this is the so called "El Padre" state (Ravelo et al., 2014), which is not a individual event, like El Niño, but a "mean state". The deepening of the thermocline and, therefore, the phenomena of El Niño, is triggered by the warming of the EEP and by the consequent drop of the temperature gradient between the Western Pacific Warm Pool and the EEP (Wara et al., 2005; Zhang et al., 2014a), consisting in a mean zonal gradient in the case of El Padre.

The hypothesis on whether the El Padre state either existed or is just a result of a bias in the proxies ($TEX_{86}$, $U^{K'}_{37}$, Mg/Ca) used for the reconstruction of the SST gradient is still ongoing (Ravelo et al., 2014; White and Ravelo 2020b; Zhang et al., 2014a, 2014b, and reference therein), also extending into the Middle Miocene (Fox et al., 2021).

Although the discussion on the existence of an El Padre State lies outside the objectives of this paper, we would like to point out that: (a) there is no doubt that the CLQ20 *Coscinodiscus* laminae point to a deepening of the thermocline in the Messinian and it is stunning to observe that the deposition of CLQ20 happened during a period when SST in the EEP were increasing (Figure 3) and (b) a primary production segregated at the thermocline depth may help explain the so-called "Pliocene paradox" (Shankle et al., 2021), which highlights enhanced primary production in the EEP despite a reduced latitudinal gradient (which, as said, would imply a deepening of the thermocline in the EEP) in the Late Miocene/Early Pliocene; and (c) the BSE images of CLQ20 highlights that shade flora can represent a huge percentage of the total diatom assemblage; therefore, given the importance of the carbon export attributable to the thriving of the shade flora at depth, the use of biogenic silica as a proxy for intensification of upwelling, as done in some researches (e.g., Fox et al., 2021; Holbourn et al., 2014. Also Esperante et al., 2015 suggest that the abundant occurrence of *Thalassionema nitzschioides* in the sediment of the Pisco Fm. suggests strong upwelling conditions) should not be used without a quantitative check of the different diatom species present in the sediment.

To conclude, it is vital to point out what climate modeling suggests us: to an increase in atmospheric $CO_2$, models point out a reduction of the temperature gradient between the Western Pacific Warm Pool and the EEP, caused by an enhanced warming of the EEP compared to the West Pacific (Meehl & Washington, 1996); as such, the current increase of $CO_2$ in the atmosphere, may lead to a future characterised by more frequent El-Niño events (Meehl & Washington, 1996).

### 4.2. The Role of Diatom Laminations in Preserving Marine Fossil Vertebrates

The investigation of diatomaceous laminae of the CLQ20 sample, the recognition of some laminae sequences that may be assumed as annual cycles (literally the mixed lamina-*Coscinodiscus* lamina and the terrigenous lamina-*Coscinodiscus* lamina duplets) and the possibility of measuring their thickness, open a further discussion on their role in favoring the preservation of marine fossils in the F member of the Pisco Fm at CLQ. The sedimentation rates registered along the F member (approximately 500 μm–2 mm/a for the mixed lamina-*Coscinodiscus* lamina duplet, Figure 5b; 900 μm for the terrigenous lamina –*Coscinodiscus* lamina duplet, Figure 8a), although

10.1029/2022PA004566

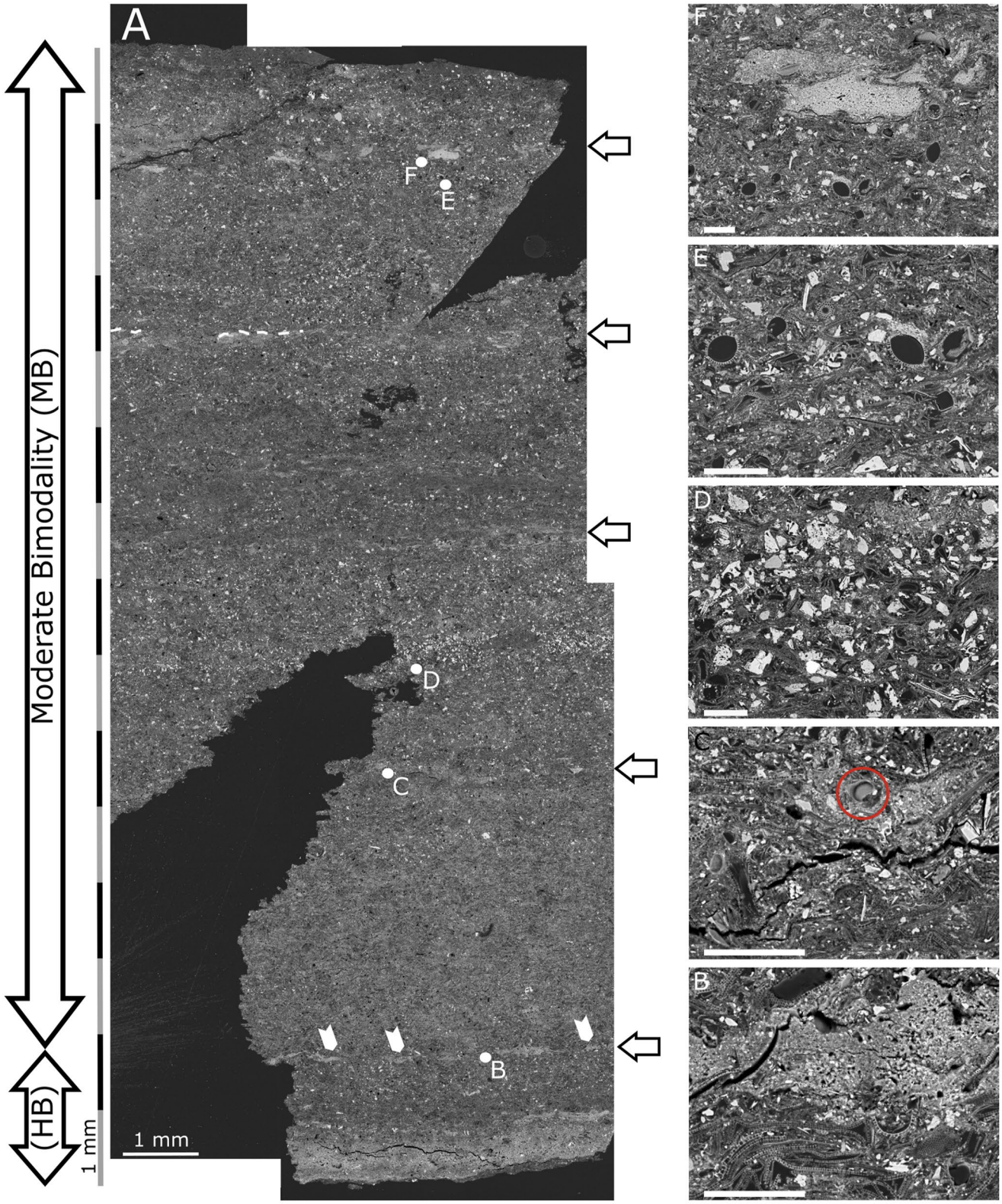


**Figure 7.**

supported by few data, are conspicuously different from those calculated for the whole section at CLQ, at least doubling and sometimes even increasing of one order of magnitude those previously reported by Gariboldi et al., 2017 (0.2 mm/a of Gariboldi et al., 2017 for the CLQ section vs. 0.5–2 mm/a (50–200 cm/ka) for the F member, this study). Differing from Gariboldi et al. (2017), who took in account a compaction of the sediments equal to 60% (by giving a wrong interpretation to Isaacs et al., 1983), in this paper we consider a definitely lower porosity loss for diatomaceous sediments due to compaction: Hamilton (1976) calculated a porosity loss during early burial of diatomaceous sediments equal to 15% (from 86% to 71% at 500 m below sea floor). Adding this 15% to the thickness of laminae observed in CLQ20 would implicate an insignificant increase to the yearly sedimentation rates. This implies that only in some cases these sedimentation rates are higher than those of Quaternary basins where primary production is high (e.g., Pleistocene of DSDP Site 478, Gulf of California, DSDP Leg 64, >125 cm/ka, Schrader, 1982; Quaternary of ODP Site 686, West Pisco Basin, ODP Leg 112, 16 cm/ka Suess et al., 1988; Pleistocene of ODP Site 1,078 outside the Bight of Angola, ODP Leg 175, 60 cm/ka, Wefer et al., 1998; Pleistocene of ODP Site 881, 5.6 cm/ka and Mio–Pliocene of ODP Site 883, 9.1 cm/ka, Subarctic Pacific Ocean, ODP Leg 145, Rea et al., 1993); to this list we add the sedimentation rates recorded in the last 2.6 ka old sediments of the Edisto Inlet, Ross Sea, Antarctica: Tesi et al. (2020) calculated a sedimentation rate equal to 2–7 mm/a (200–700 cm/ka) for the laminated diatomaceous sediment of core HLF17-01. As, due to their lithology and fabric, diatomaceous sediments of the Edisto Inlet may be considered a modern analogue of sediments from the F member, it is worth reporting that in core ANTA02-CH41, Edisto Inlet, the soupy consistence of the diatomaceous laminated mud revealed a water content that was close to 80% (Finocchiaro et al., 2005). Imaging such physical characteristic for a just-deposed diatom ooze at the bottom of the East Pisco Basin would itself explain how deep marine vertebrate carcasses may have sunk into the sediments, supporting the "impact burial" (partial or complete burial of an object in the sediments upon its high velocity sinking through the water column into soupy substrates) hypothesis proposed by Bosio et al. (2021a) to explain the rapid burial of marine vertebrates in the Pisco Fm. Indeed, any of the sedimentation rates calculated in this paper and in Gariboldi et al., 2017 are not high enough to cover large carcasses permitting high articulation and high completeness of the fossil specimens, as observed in the Pisco Fm (Gariboldi et al., 2015). As such, we agree with Brand et al. (2004), who state that rapid burial is needed to explain such a preservation in the Pisco Fm. However, we disagree when they state that "such burial requires diatom accumulation rates at least three to four orders of magnitude faster than is usual in the ocean today—centimeters per week or month, rather than centimeters per thousand years." Also, Gariboldi et al. (2015) highlighted the role of dolomite precipitation inside and outside (dolomite nodule) the whale carcasses in the process of preservation of the fossils (e.g., by avoiding bone dissolution, preventing diagenetic compression of the specimens and erosion of bones, favoring the articulation and completeness of skeletons). The process of dolomite precipitation, which also includes recurrent basin-wide decimetric-thick dolomite layers (Malinverno et al., 2023), was explained as biomediated by sulfate-reducing bacteria, which are able to degrade organic matter in low-oxygen environment, as demonstrated also in laboratory experiments (see references therein Gariboldi et al., 2015). Thus, the sinking of the carcasses into the soupy diatom ooze would have favored the formation of the Pisco Lagerstätte also by subtracting the carcasses from a possible oxygenated sea floor, thus favoring dolomite precipitation.

### 4.3. CLQ20: That's One Small Sample for a Formation

We need to recall to the readers that the CLQ20 sample is a very short piece of the diatomite portion of the P2 allomember of the Pisco Fm and that it may be representative neither of the whole F member, nor of the diatomitic portions of the other older and younger allomembers of the Pisco Fm (Lamy et al., 2001, affirm that changes in continental rainfall in southern Chile are regulated by millennial to multi-centennial shifts in the position of the southern westerlies, periods that lag far behind the duration of the CLQ F member deposition). However, in their studies of the biostratigraphy of the Pisco Fm, Gariboldi et al. (2017) have published a table

**Figure 7.** BSE-SEM images of slide t9. (a) Low magnification (100x) BSE image of slide t9, which is characterized at its bottom by a high bimodality, given by the contrast of a terrigenous lamina and the terrigenous boudinage-like top of a mixed lamina (arrowheads) with the overlying biogenic laminae (see panel b; Figure 8a). The rest of the slide is characterized by moderate bimodality given by the sparse presence of silt particles in mixed laminae, which alternates with *Coscinodiscus* laminae (see Figure S2 in Supporting Information S1) within a darker matrix (diatomite). White arrows indicate the thin terrigenous boudinage-like top of the mixed laminae. The dotted line represents a continuous, straight but faint, upper boundary between the terrigenous top of a mixed lamina with a *Coscinodiscus* lamina. Letters highlights the position of images in the right column. (b) Lower boundary of the terrigenous top of a mixed lamina. (c) Detail of a diatom valve (red circle) within the terrigenous top of the mixed lamina. (d) Silt particles in a mixed lamina. (e) *Stephanopyxis* frustules within a mixed lamina. (f) Boudinage-like structure of the terrigenous top of a mixed lamina. Scale bars in panels b–f: 100 μm.

10.1029/2022PA004566

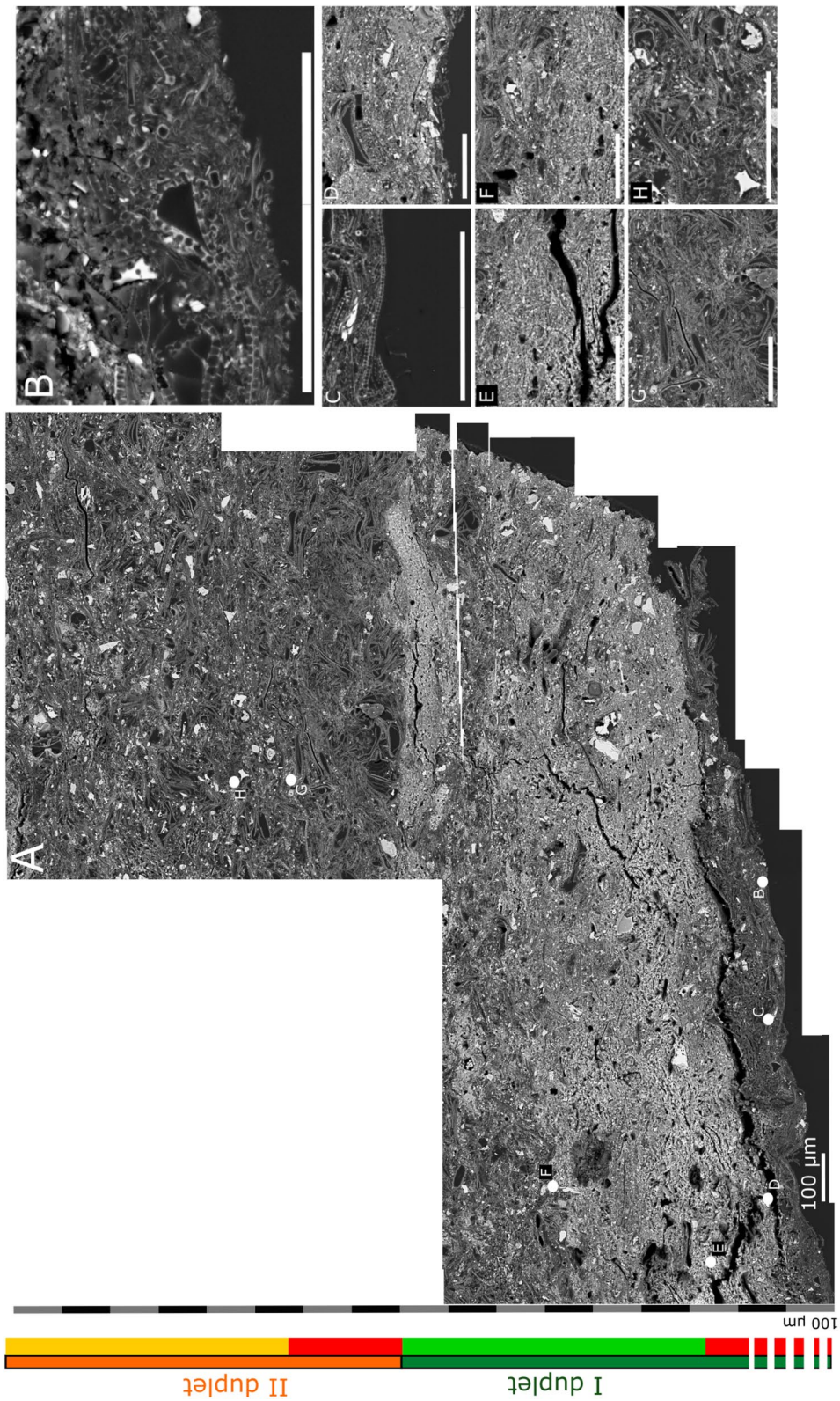


**Figure 8.** BSE-SEM images of slide t9. (a) High magnification (2000x) BSE image of the bottom of slide t9 (the same visible in panel Figure 7a). Letters highlights the position of images in panels (b–h). (b) Details of *Thalassionema* specimens within a *Coscinodiscus* lamina. (c) Silt particle within a *Coscinodiscus* lamina. (d) Detail of sparse diatom frustules within a terrigenous lamina. (e) Detail of a terrigenous lamina. (f) Boundary between a terrigenous lamina with the overlying *Coscinodiscus* lamina. The boundary is wavy and interdigitated. (g) Boundary between a *Coscinodiscus* lamina with the overlying mixed lamina. The boundary is wavy, and faint, but continuous. (h) *Chaetoceros Hyalochaete* resting spores within a mixed lamina. Scale bars in b–h: 100 µm.

**Table 1**
*Ecology of Principal Diatom Genera and Species Listed in This Paper*

| Genus/Species | Ecology |
|---|---|
| *Actinocyclus octonarius* Ehrenberg, 1837 | Meroplanktic species correlated with the distribution of *Coscinodiscus*, Schuette and Schrader (1981b) |
| *Actinoptychus senarius* (Ehrenberg) Ehrenberg 1843 | Neritic, Cupp (1943); typical of coastal upwelling assemblages, Abrantes et al. (2007) |
| *Chaetoceros* Ehrenberg, 1844 *Hyalochaete* Gran (1897) spp. RS | A truly planktic genus. Most of *Chaetoceros* species are neritic, although some are oceanic. No fresh-water species are known, Cupp (1943). *Chaetoceros* RS form at the end of upwelling bloom (spring and autumn), when the surface waters are depleted in nutrients: Schuette and Schrader (1981a, 1981b); Kemp et al. (2000); Romero and Hebbeln (2003) |
| Coscinodiscus *Ehrenberg*, 1839, nom. et typ. cons | Recorded in modern environments as repeatedly forming continuous belts and patches, Schuette and Schrader (1981b). Thrives at the thermo/nutricline at low light conditions, prefers a stratified water column (part of the "shade flora"): Sournia (1982); Kemp et al. (2000) |
| *Coscinodiscus asteromphalus* Ehrenberg, 1844 | *C. asteromphalus* tolerates a wide range of temperatures and may be cosmopolitan, Hasle and Syvertsen (1997) |
| *Stephanopyxis turris* (Greville) Ralfs 1861 | Neritic, temperate and subtropical species, Cupp (1943) |
| *Thalassionema* Grunow ex Mereschkowsky, 1902 | A common marine plankton genus, Round et al. (1990) |
| *Thalassionema nitzshioides* (Grunow) Mereschkowsky, 1902 | Marine, neritic and estuarine species; euryhaline and eurythermal, Navarro (1982). It blooms in spring and summer, Schuette and Schrader (1981a). *Thalassionema nitzschioides* var. *nitzschioides* is classified as part of the coastal upwelling group by Romero and Hebbeln (2003) |

of relative abundances for all the diatom species encountered in the CLQ; from this work (Table 3 of Gariboldi et al., 2017; see Text S3 in Supporting Information S1) we can infer that *Coscinodiscus asteromphalus* is present in great abundance in almost all the samples collected in the CLQ F member; yet, also CRS are always present. This apparent equality between these two genera abundances can be explained considering the counting method (Armand, 1997; Crosta & Koç, 2007; Schrader & Gersonde, 1978); following this protocol only *Coscinodicus* spp. valve which are preserved for ¾ or more can be counted in the assemblage. However, the higher valve-face diameter/pervalvar-axis ratio makes large diatoms easier to break during slide preparation, resulting at last in an underestimation of large diatoms in the assemblages. Conversely CRS are often found intact, with the 2 valves still connected.

As such, it appears clear that analyses on diatom assemblages by means of the light miscroscope, combined with those on diatom laminations, where possible, may be the most direct proxy, yet imprecise (as they give no absolute values on the reduced zonal SST gradient), to study the initiation and the temporal patterns of ENSO in the deep time and to verify the hypothesis of the El Padre state. The observation of laminae in their original depositional settings gives a glimpse, not only on the depositional mechanism, but also on the real relative abundance of different species; light microscope analysis is essential to investigate long stratigraphic succession efficiently.

## 5. Conclusions

Backscattered electron imagery analysis of CLQ laminated diatomaceous mudstone provided insight into the seasonality that was affecting water column stability.

The most frequent laminae duplet observed in the Messinian CLQ20 sample is the mixed lamina—*Coscinodiscus* lamina duplet. The large contribution in the CLQ20 sediments of this duplet, and of the genus *Coscinodiscus* in general (also in the less frequent terrigenous lamina—*Coscinodiscus* lamina duplet), reflects a rather deep position of the thermocline. This water column setup led to a weak proliferation of upwelling related diatom species (i.e., *Chaetoceros Hyalochaete* and *Thalassionema*), as the upwelled waters were warm and nutrient-poor. Such oceanographic situation resembles that hypothesized for the so-called "El Padre" state in the middle Pliocene Warm Period; this is described as a constant El Niño phenomenon (a "mean state") triggered by the warming of the EEP and the consequent drop of the temperature gradient between the West Pacific Warm Pool and the EEP itself. As such, we highlight that: (a) studies focused on verifying the existence of the El Padre setup in the low latitude Pacific during the Late Miocene are needed; and (b) climate modeling suggests that to a future increase

in atmospheric $CO_2$ will correspond an enhanced warming of the EEP compared to the West Pacific, which may lead to more frequent El-Niño events.

Analyses on CLQ20 laminae thickness have confirmed that sedimentation rates in the Pisco Basin during the Late Miocene were comparable to those of Quaternary basins elsewhere. This evidence rules out the hypothesis that depositions of diatomites in the East Pisco Basin were orders magnitude faster than in today's oceans. Moreover, direct observation on modern diatom oozes and the observation made on their water content, make us affirm that the hypothesis of an "impact burial" for the marine vertebrate carcasses is robust.

On a broader view, our study suggests that.

1. During diatom counts for palaecological analysis, special care should be paid in not underestimating large-sized diatoms over small-sized ones; light microscope analysis coupled with BSEI analysis on diatom laminations (where possible) helps overcome this possible bias;
2. Analyses on diatom assemblages and diatom laminations, where possible, may be the most direct proxy, yet imprecise (as it gives no absolute values on the reduced zonal SST gradient), to study ENSO in the deep time;
3. The use of biogenic silica as a proxy for intensification of upwelling, as done in some researches, should be used with caution, given the importance of the carbon export attributable to the thriving of the shade flora at depth.

## Data Availability Statement

BSE images are from Gariboldi et al., 2023. Data used to compile Figure 3 are available from Rousselle et al., 2013 and Herbert et al., 2016.

**Acknowledgments**
We would like to thank Anthony Oldroy, Peter Fisher, Lindsey Axe and Duncan Muir (School of Earth and Environmental Sciences, Cardiff University) for the help during sample preparation and SEM analyses. We would also like to thank Prof. John Barron and Prof. C. Lange for their constant support and for the many productive discussions. This study was supported by Grants from the Italian Ministero dell'Istruzione dell'Università e della Ricerca (PRIN Project 2012YJSBMK to G. Bianucci), by a National Geographic Society Committee for Research Exploration Grants (9410-13 to G. Bianucci), and the University of Camerino (FAR 2019; STI000102 to C. Di Celma). K.G. would like to thank Caterina Morigi, Alessandra Negri and Giacomo Galli for their help in improving the manuscript. We would like to thank the Editor, Ursula Röhl, Associated Editor, Alex Farnsworth, and the anonymous Reviewers for the precious observations that have helped us improving the manuscript and Editor's Assistant, Meghan Ramil, for the technical assistance during the peer-review process. This work is dedicated to those we lost during the COVID-19 pandemic.

## References

Abrantes, F., Lopes, C., Mix, A., & Pisias, N. (2007). Diatoms in Southeast Pacific surface sediments reflect environmental properties. *Quaternary Science Reviews*, *26*(1–2), 155–169. https://doi.org/10.1016/j.quascirev.2006.02.022

Adamson, G. (2019). El Niño and society. In *Oxford research encyclopedia of climate science*. Oxford University Press.

Alley, K., Patacca, K., Pike, J., Dunbar, R., & Leventer, A. (2018). Iceberg alley, East Antarctic margin: Continuously laminated diatomaceous sediments from the late Holocene. *Marine Micropaleontology*, *140*, 56–68. https://doi.org/10.1016/j.marmicro.2017.12.002

Armand, L. (1997). *The use of diatom transfer functions in estimating sea-surface temperature and sea-ice in cores from the southeast Indian Ocean*. Ph.D thesis. Australian National University.

Bianucci, G., Di Celma, C., Collareta, A., Landini, W., Post, K., Tinelli, C., et al. (2016). Fossil marine vertebrates of Cerro Los Quesos: Distribution of cetaceans, seals, crocodiles, seabirds, sharks, and bony fish in a late Miocene locality of the Pisco Basin, Peru. *Journal of Maps*, *12*(5), 1037–1046. https://doi.org/10.1080/17445647.2015.1115785

Bianucci, G., Di Celma, C., Landini, W., Post, K., Tinelli, C., de Muizon, C., et al. (2016). Distribution of fossil marine vertebrates in Cerro Colorado, the type locality of the giant raptorial sperm whale Livyatanmelvillei (Miocene, Pisco Formation, Peru). *Journal of Maps*, *12*(3), 543–557. https://doi.org/10.1080/17445647.2015.1048315

Bosio, G., Collareta, A., Di Celma, C., Lambert, O., Marx, F. G., de Muizon, C., et al. (2021a). Taphonomy of marine vertebrates of the Pisco Formation (Miocene, Peru): Insights into the origin of an outstanding fossil-lagerstätte. *PLoS One*, *16*(7), e0254395. https://doi.org/10.1371/journal.pone.0254395

Bosio, G., Gioncada, A., Gariboldi, K., Bonaccorsi, E., Collareta, A., Pasero, M., et al. (2021b). Mineralogical and geochemical characterization of fossil bones from a Miocene marine Konservat-Lagerstätte. *Journal of South American Earth Sciences*, *105*, 102924. https://doi.org/10.1016/j.jsames.2020.102924

Brand, L., Urbina, M., Chadwick, A., DeVries, T. J., & Esperante, R. (2011). A high resolution stratigraphic framework for the remarkable fossil cetacean assemblage of the Miocene/Pliocene Pisco Formation, Peru. *Journal of South American Earth Sciences*, *31*(4), 414–425. https://doi.org/10.1016/j.jsames.2011.02.015

Brand, L. R., Esperante, R., Chadwick, A. V., Poma Porras, O., & Alomía, M. (2004). Fossil whale preservation implies high diatom accumulation rate in the Miocene-Pliocene Pisco Formation of Peru. *Geology*, *32*(2), 165–168. https://doi.org/10.1130/g20079.1

Briceño-Zuluaga, F. J., Sifeddine, A., Caquineau, S., Cardich, J., Salvatteci, R., Gutierrez, D., et al. (2016). Terrigenous material supply to the Peruvian central continental shelf (Pisco, 14°S) during the last 1,000 years: Paleoclimatic implications. *Climate of the Past*, *12*(3), 787–798. https://doi.org/10.5194/cp-12-787-2016

Brodie, I., & Kemp, A. E. S. (1994). Variation in biogenic and detrital fluxes and formation of laminae in late Quaternary sediments from the Peruvian coastal upwelling zone. *Marine Geology*, *116*(3–4), 385–398. https://doi.org/10.1016/0025-3227(94)90053-1

Bull, D., Kemp, A. E. S., & Weedon, G. P. A. (2000). 160-k.y.-old-record of El Niño southern Oscillation in marine production and coastal run-off from Santa Barbara Basin, California, USA. *Geology*, *28*(11), 1007–1010. https://doi.org/10.1130/0091-7613(2000)028<1007:akyoro>2.3.co;2

Caviedes, C. N. (1984). El Nino 1982-83. *Geographical Review*, *74*(3), 267–290. https://doi.org/10.2307/214939

Collareta, A., Lambert, O., Marx, F. G., de Muizon, C., Varas-Malca, R., Landini, W., et al. (2021). Vertebrate palaeoecology of the Pisco Formation (Miocene, Peru): Glimpses into the ancient humboldt current ecosystem. *Journal of Marine Science and Engineering*, *9*(11), 1188. https://doi.org/10.3390/jmse9111188

Collareta, A., Landini, W., Lambert, O., Post, K., Tinelli, C., Di Celma, C., et al. (2015). Piscivory in a Miocene Cetotheriidae of Peru: First record of fossilised stomach content for an extinct baleen-bearing whale. *Science and Nature*, *102*(11–12), 70. https://doi.org/10.1007/s00114-015-1319-y

Corselli, C., Principato, M. S., Maffioli, P., & Crudeli, D. (2002). Changes in planktonic assemblages during sapropel S5 deposition: Evidence from Urania Basin area, eastern Mediterranean. *Paleoceanography*, *17*(3), 1–30. https://doi.org/10.1029/2000pa000536

Crosta, X., & Koç, N. (2007). Chapter eight diatoms: From micropaleontology to isotope geochemistry. *Developments in Marine Geology*, *1*, 327–369.

Cupp, E. E. (1943). *Marine plankton diatoms of the west coast of North America*. Otto Koeltz Science Publishers.

Davies, A., & Kemp, A. E. (2016). Late Cretaceous seasonal palaeoclimatology and diatom palaeoecology from laminated sediments. *Cretaceous Research*, *65*, 82–111. https://doi.org/10.1016/j.cretres.2016.04.014

Davies, A., Kemp, A. E., & Pike, J. (2009). Late Cretaceous seasonal ocean variability from the Arctic. *Nature*, *460*(7252), 254–258. https://doi.org/10.1038/nature08141

Davies, A., Kemp, A. E., Weedon, G. P., & Barron, J. A. (2012). El Niño–southern oscillation variability from the late cretaceous Marca shale of California. *Geology*, *40*(1), 15–18. https://doi.org/10.1130/g32329.1

De Muizon, C., & DeVries, T. J. (1985). Geology and paleontology of late Cenozoic marine deposits in the Sacaco area (Peru). *Geologische Rundschau*, *74*(3), 547–563. https://doi.org/10.1007/bf01821211

DeVries, T. J. (1988). Paleoenvironments of the Pisco Basin. Cenozoic geology of the Pisco Basin. In R. B. Dunbar & P. A. Baker (Eds.), *Guidebook, IGCP 156 field workshop: Genesis of cenozoic phosphorites and associated organic-rich sediments: Peruvian continental margin* (pp. 41–50).

Di Celma, C., Malinverno, E., Cantalamessa, G., Gioncada, A., Bosio, G., Villa, I. M., et al. (2016). Stratigraphic framework of the late Miocene Pisco Formation at Cerro Los Quesos (Ica Desert, Peru). *Journal of Maps*, *12*(5), 1020–1028. https://doi.org/10.1080/17445647.2015.1115783

Drebes, G. (1966). On the life history of the marine plankton diatom *Stephanopyxis palmeriana*. *Helgoländer wissenschaftliche Meeresuntersuchungen*, *13*(1), 101–114. https://doi.org/10.1007/bf01612659

Dunbar, R. B., & Berger, W. H. (1981). Fecal pellet flux to modern bottom sediment of Santa Barbara Basin (California) based on sediment trapping. *Geological Society of America Bulletin*, *92*(4), 212–218. https://doi.org/10.1130/0016-7606(1981)92<212:fpftmb>2.0.co;2

Dunbar, R. B., Marty, R. C., & Baker, P. A. (1990). Cenozoic marine sedimentation in the Sechura and Pisco basins, Peru. *Palaeogeography, Palaeoclimatology, Palaeoecology*, *77*(3–4), 235–261. https://doi.org/10.1016/0031-0182(90)90179-b

Esperante, R., Brand, L., Nick, K., Poma, O., & Urbina, M. (2008). Exceptional occurrence of fossil baleen in shallow marine sediments of the Neogene Pisco Formation, Southern Peru. *Palaeogeography, Palaeoclimatology, Palaeoecology*, *257*(3), 344–360. https://doi.org/10.1016/j.palaeo.2007.11.001

Esperante, R., Brand, L. R., Chadwick, A. V., & Poma, O. (2015). Taphonomy and paleoenvironmental conditions of deposition of fossil whales in the diatomaceous sediments of the Miocene/Pliocene Pisco Formation, southern Peru—A new fossil-lagerstätte. *Palaeogeography, Palaeoclimatology, Palaeoecology*, *417*, 337–370. https://doi.org/10.1016/j.palaeo.2014.09.029

Fedorov, A. V., Dekens, P. S., McCarthy, M., Ravelo, A. C., DeMenocal, P. B., Barreiro, M., et al. (2006). The Pliocene paradox (mechanisms for a permanent El Niño). *Science*, *312*(5779), 1485–1489. https://doi.org/10.1126/science.1122666

Finocchiaro, F., Langone, L., Colizza, E., Fontolan, G., Giglio, F., & Tuzzi, E. (2005). Record of the early holocene warming in a laminated sediment core from cape Hallett bay (northern Victoria Land, Antarctica). *Global and Planetary Change*, *45*(1–3), 193–206. https://doi.org/10.1016/j.gloplacha.2004.09.003

Fox, L. R., Wade, B. S., Holbourn, A., Leng, M. J., & Bhatia, R. (2021). Temperature gradients across the Pacific Ocean during the middle Miocene. *Paleoceanography and Paleoclimatology*, *36*(6), e2020PA003924. https://doi.org/10.1029/2020pa003924

Gariboldi, K., Bosio, G., Malinverno, E., Gioncada, A., Di Celma, C., Villa, I. M., et al. (2017). Biostratigraphy, geochronology and sedimentation rates of the upper Miocene Pisco Formation at two important marine vertebrate fossil-bearing sites of southern Peru. *Newsletters on Stratigraphy*, *50*(4), 417–444. https://doi.org/10.1127/nos/2017/0345

Gariboldi, K., Gioncada, A., Bosio, G., Malinverno, E., Di Celma, C., Tinelli, C., et al. (2015). The dolomite nodules enclosing fossil marine vertebrates in the East Pisco basin, Peru: Field and petrographic insights into the lagerstätte formation. *Palaeogeography, Palaeoclimatology, Palaeoecology*, *438*, 81–95. https://doi.org/10.1016/j.palaeo.2015.07.047

Gariboldi, K., Pike, J., Malinverno, E., Di Celma, C., Gioncada, A., & Bianucci, G. (2023). BSE images of sample CLQ20, laminated diatomites, Upper Miocene Pisco Fm, Peru. [Dataset]. Figshare. https://doi.org/10.6084/m9.figshare.22309204.v1

Gioncada, A., Collareta, A., Gariboldi, K., Lambert, O., Di Celma, C., Bonaccorsi, E., et al. (2016). Inside baleen: Exceptional microstructure preservation in a late Miocene whale skeleton from Peru. *Geology*, *44*(10), 839–842. https://doi.org/10.1130/g38216.1

Gioncada, A., Gariboldi, K., Collareta, A., Di Celma, C., Bosio, G., Malinverno, E., et al., (2018a). Looking for the key to preservation of fossil marine vertebrates in the Pisco Formation of Peru: New insights from a small dolphin skeleton. *Andean Geology*, *45*(3), 379–398. https://doi.org/10.5027/andgeov45n3-3122

Gioncada, A., Petrini, R., Bosio, G., Gariboldi, K., Collareta, A., Malinverno, E., et al. (2018b). Insights into the diagenetic environment of fossil marine vertebrates of the Pisco Formation (late Miocene, Peru) from mineralogical and Sr-isotope data. *Journal of South American Earth Sciences*, *81*, 141–152. https://doi.org/10.1016/j.jsames.2017.11.014

Grigorov, I., Pearce, R. B., & Kemp, A. E. S. (2002). Southern Ocean laminated diatom ooze: Mat deposits and potential for palaeo-flux studies, ODP leg 177, site 1093. *Deep-Sea Research*, *49*(16), 3391–3407. https://doi.org/10.1016/s0967-0645(02)00089-9

Grimm, K. A., Lange, C. B., & Gill, A. S. (1996). Biological forcing of hemipelagic sedimentary laminae; evidence from ODP Site 893, Santa Barbara Basin, California. *Journal of Sedimentary Research*, *66*(3), 613–624.

Hamilton, E. L. (1976). Variations of density and porosity with depth in deep-sea sediments. *Journal of Sedimentary Research*, *46*(2), 280–300.

Hasle, G. R., Syvertsen, E. E., Steidinger, K. A., Tangen, K., Throndsen, J., & Heimdal, B. R. (1997). Identification of marine phytoplankton.

Hebbeln, D., Marchant, M., & Wefer, G. (2000). Seasonal variations of the particle flux in the Peru-Chile current at 30 S under "normal"and El Niño conditions. *Deep Sea Research Part II: Topical Studies in Oceanography*, *47*(9–11), 2101–2128. https://doi.org/10.1016/s0967-0645(00)00018-7

Herbert, T. D., Lawrence, K. T., Tzanova, A., Peterson, L. C., Caballero-Gill, R., & Kelly, C. S. (2016). Late Miocene global cooling and the rise of modern ecosystems. *Nature Geoscience*, *9*(11), 843–847. https://doi.org/10.1038/NGEO2813

Hill, A. E., Hickey, B. M., Shillington, F. A., Strub, P. T., Brink, K. H., Barton, E. D., & Thomas, A. C. (1998). Eastern Ocean boundaries. In A. R. Robinson & K. H. Brink (Eds.), *The Sea* (Vol. 11, pp. 29–67). John Wiley and Sons Edition.

Holbourn, A., Kuhnt, W., Lyle, M., Schneider, L., Romero, O., & Andersen, N. (2014). Middle Miocene climate cooling linked to intensification of eastern equatorial Pacific upwelling. *Geology*, *42*(1), 19–22. https://doi.org/10.1130/g34890.1

Hsu, J. T. (1992). Quaternary uplift of the Peruvian coast related to the subduction of the Nazca ridge: 13.5–15.6 degrees south latitude. *Quaternary International*, *15–16*, 87–97. https://doi.org/10.1016/1040-6182(92)90038-4

Huyer, A., Smith, R. L., & Paluszkiewicz, T. (1987). Coastal upwelling off Peru during normal and El Niño times, 1981–1984. *Journal of Geophysical Research*, *92*(C13), 14297–14307. https://doi.org/10.1029/jc092ic13p14297

Isaacs, C. M., Pisciotto, K. A., & Garrison, R. E. (1983). Facies and diagenesis of the Miocene monterey formation, California: A summary. *Developments in Sedimentology*, *36*, 247–282.
Kemp, A. E. S. (1990). Sedimentary fabrics and variation in lamination style in Peru continental margin upwelling sediments. *Proceedings of ODP, Scientific Results*, *112*, 43–58.
Kemp, A. E. S., Pearce, R. B., Koizumi, I., Pike, J., & Rance, S. J. (1999). The role of mat-forming diatoms in formation of the Mediterranean sapropels. *Nature*, *398*(6722), 57–61. https://doi.org/10.1038/18001
Kemp, A. E. S., Pike, J., Pearce, R. B., & Lange, C. B. (2000). The "Fall dump"-a new perspective on the role of a "shade flora" in the annual cycle of diatom production and export flux. *Deep-Sea Research II*, *47*(9–11), 2129–2154. https://doi.org/10.1016/s0967-0645(00)00019-9
Lambert, O., Bianucci, G., Post, K., de Muizon, C., Salas-Gismondi, R., Urbina, M., & Reumer, J. (2010). The giant bite of a new raptorial sperm whale from the Miocene epoch of Peru. *Nature*, *466*(7302), 105–108. https://doi.org/10.1038/nature09067
Lamy, F., Hebbeln, D., Röhl, U., & Wefer, G. (2001). Holocene rainfall variability in southern Chile: A marine record of latitudinal shifts of the southern westerlies. *Earth and Planetary Science Letters*, *185*(3–4), 369–382. https://doi.org/10.1016/s0012-821x(00)00381-2
Liu, Z., & Herbert, T. D. (2004). High-latitude influence on the eastern equatorial Pacific climate in the early Pleistocene epoch. *Nature*, *427*(6976), 720–723. https://doi.org/10.1038/nature02338
Maddison, E. J., Pike, J., & Dunbar, R. (2012). Seasonally laminated diatom-rich sediments from Dumont d'Urville trough, East Antarctic margin: Late-holocene neoglacial sea-ice conditions. *The Holocene*, *22*(8), 857–875. https://doi.org/10.1177/0959683611434223
Malinverno, E., Bosio, G., Gioncada, A., Cimò, R., Andò, S., Mariani, L., et al. (2023). Laterally-continuous dolomite layers of the Miocene Pisco Formation (East Pisco basin, Peru): A window into past cyclical changes of the diagenetic environment. *Marine and Petroleum Geology*, *147*, 105977. https://doi.org/10.1016/j.marpetgeo.2022.105977
Marty, R. (1988). *Stratigraphy and chemical sedimentology of Cenozoic biogenic sediments from the Pisco and Sechura Basins, Peru*. PhD Thesis. Rice University.
Marx, F. G., & Uhen, M. D. (2010). Climate, critters, and cetaceans: Cenozoic drivers of the evolution of modern whales. *Science*, *327*(5968), 993–996. https://doi.org/10.1126/science.1185581
Meehl, G. A., & Washington, W. M. (1996). El Niño-like climate change in a model with increased atmospheric CO 2 concentrations. *Nature*, *382*(6586), 56–60. https://doi.org/10.1038/382056a0
Molina, R. E., Manrique, F. A., & García, J. (1997). Nota sobre un florecimiento de *Stephanopyxis palmeriana* (Greville) Grunow (Bacillariophyceae) en la bahía Kun Kaak, Golfo de California. *Hidrobiologica*, *7*(1), 84–86.
Montoya, M., García, W., & Vidal, J. C. (1994). *Geología de los cuadrángulos de Lomitas, palpa, nasca y puquio: Hojas 30-l, 30-m, 30-n, 30-ñ*. Instituto Geológico Minero y Metalúrgico.
Müller, P. J., Kirst, G., Ruhland, G., Von Storch, I., & Rosell-Melé, A. (1998). Calibration of the alkenone paleotemperature index U37K' based on core-tops from the eastern South Atlantic and the global ocean (60 N–60 S). *Geochimica et Cosmochimica Acta*, *62*(10), 1757–1772. https://doi.org/10.1016/s0016-7037(98)00097-0
Navarro, J. N. (1982). A survey of the marine diatoms of Puerto Rico. In *IV. Suborder araphidineae: Families diatomaceae and protoraphidaceae* (Vol. 24). Botanica Marina.
Palmer, A. A., Austin, J. A., Jr., & Schlager, W. (1986). Introduction and explanatory notes. *Proceedings of ODP, Scientific Results*, *101*, 5–23.
Pike, J., Bernhard, J. M., Moreton, S. G., & Butler, I. B. (2001). Microbioirrigation of marine sediments in dysoxic environments: Implications for early sediment fabric and diagenetic processes. *Geology*, *29*(10), 923–926. https://doi.org/10.1130/0091-7613(2001)029<0923:momsid>2.0.co;2
Pike, J., & Kemp, A. E. S., (1996a). Preparation and analysis techniques for studies of laminated sediments. In A. E. S. Kemp (Ed.) *Palaeoclimatology and Palaeooceanography from laminated sediments* (Vol. 116, pp. 37–48). Geological Society Special Publication.
Pike, J., & Kemp, A. E. S., (1996b). Records of seasonal flux in Holocene laminated sediments, Gulf of California. In A. E. S. Kemp (Ed.) *Palaeoclimatology and Palaeooceanography from laminated sediments* (Vol. 116, pp. 157–170). Geological Society Special Publication.
Pike, J., & Kemp, A. E. S. (1997). Early Holocene decadal-scale ocean variability recorded in Gulf of California laminated sediments. *Paleoceanography*, *12*(2), 227–238. https://doi.org/10.1029/96pa03132
Pike, J., & Kemp, A. E. S. (1999). Diatom mats in Gulf of California sediments: Implication for the paleoenvironmental interpretation of laminated sediments and silica burial. *Geology*, *27*(4), 311–314. https://doi.org/10.1130/0091-7613(1999)027<0311:dmigoc>2.3.co;2
Pike, J., & Stickley, C. E. (2013). Diatom fossil record from marine laminated sediments. In S. By, Elias, & C. Mock (Eds.), *Encyclopedia of quaternary science* (Vol. 1, pp. 554–561).
Pilskaln, C. H., & Pike, J. (2001). Formation of Holocene sedimentary laminae in the Black Sea and the role of the benthic flocculent layer. *Paleoceanography*, *16*, 1–19. https://doi.org/10.1029/1999pa000469
Ragaini, L., Di Celma, C., & Cantalamessa, G. (2008). Warm-water mollusc assemblages from northern Chile (Mejillones Peninsula): New evidence for permanent El Niño-like conditions during Pliocene warmth? *Journal of the Geological Society*, *165*(6), 1075–1084. https://doi.org/10.1144/0016-76492007-039
Ravelo, A. C., Deken, P. S., & McCarthy, M. (2006). Evidence for El Niño-like conditions during the Pliocene. *Geological Society of America Today*, *16*(3), 4. https://doi.org/10.1130/1052-5173(2006)016<4:efenlc>2.0.co;2
Ravelo, A. C., Lawrence, K. T., Fedorov, A., & Ford, H. L. (2014). Comment on "A 12-million-year temperature history of the tropical Pacific Ocean". *Science*, *346*(6216), 1467. https://doi.org/10.1126/science.1257618
Rea, D. K., Basov, I. A., Janecek, T. R., & Palmer-Julson, A. (1993). Proceedings of the Ocean Drilling Program. Initial Reports 145. Ocean Drilling Program.
Romero, O., & Hebbeln, D. (2003). Biogenic silica and diatom thanatocoenosis in surface sediments below the Peru–Chile current: Controlling mechanisms and relationship with productivity of surface waters. *Marine Micropaleontology*, *48*(1–2), 71–90. https://doi.org/10.1016/s0377-8398(02)00161-5
Romero, O., Lange, C., & Hebbeln, D. (2002). Effects of El Niño 1997-98 on particle fluxes from two coastal upwelling areas: Northern Chile and southern California. *Investigaciones Marinas*, *30*(1), 172–173. https://doi.org/10.4067/s0717-71782002030100067
Round, F. E., Crawford, R. M., & Mann, D. G. (1990). *Diatoms: Biology and morphology of the genera*. Cambridge University Press.
Rousselle, G., Beltran, C., Sicre, M. A., Raffi, I., & De Rafelis, M. (2013). Changes in sea-surface conditions in the Equatorial Pacific during the middle Miocene–Pliocene as inferred from coccolith geochemistry. *Earth and Planetary Science Letters*, *361*, 412–421. https://doi.org/10.1016/j.epsl.2012.11.003
Sancetta, C. (1995). Diatoms in the Gulf of California: Seasonal flux patterns and the sediment record for the last 15,000 years. *Paleoceanography*, *10*(1), 67–84. https://doi.org/10.1029/94pa02796

Schrader, H. (1982). Diatom biostratigraphy and laminated diatomaceous sediments from the Gulf of California deep sea Drilling Project leg 64. Part A: Initial Reports. In J. R. Curray, D. G. More, K. Kelts, & G. Einsele (Eds.) *Proceedings of the ocean drilling program* (Vol. *64*, (2), pp. 1089–1116).

Schrader, H. J., & Gersonde, R. (1978). Diatoms and silicoflagellates. In A. Zachariasse, W. R. Riedel, A. Sanfilippo, R. R. Schmidt, M. J. Brolsma, H. J. Schrader, et al. (Eds.), *Micropaleontological counting methods and techniques — an exercise on an eight meters section of the Lower Pliocene of Capo Rossello, Sicily* (Vol. 17, pp. 129–176). Utrecht Micropaleontology Bulletin.

Schuette, G., & Schrader, H. (1981a). Diatom taphocoenoses in the coastal upwelling area off South West Africa. *Marine Micropaleontology*, *6*(2), 131–155. https://doi.org/10.1016/0377-8398(81)90002-5

Schuette, G., & Schrader, H. (1981b). Diatoms in surface sediments: A reflection of coastal upwelling. *Coastal upwelling*, *1*, 372–380.

Seki, O., Schmidt, D. N., Schouten, S., Hopmans, E. C., Sinninghe Damsté, J. S., & Pancost, R. D. (2012). Paleoceanographic changes in the eastern equatorial Pacific over the last 10 myr. *Paleoceanography*, *27*(3), PA3224. https://doi.org/10.1029/2011pa002158

Shankle, M. G., Burls, N. J., Fedorov, A. V., Thomas, M. D., Liu, W., Penman, D. E., et al. (2021). Pliocene decoupling of equatorial Pacific temperature and pH gradients. *Nature*, *598*(7881), 457–461. https://doi.org/10.1038/s41586-021-03884-7

Shipe, R. F., Passow, U., Brzezinski, M. A., Graham, W. M., Pak, D. K., Siegel, D. A., & Alldredge, A. L. (2002). Effects of the 1997–98 El Niño on seasonal variations in suspended and sinking particles in the Santa Barbara basin. *Progress in Oceanography*, *54*(1–4), 105–127. https://doi.org/10.1016/s0079-6611(02)00045-9

Sournia, A. (1982). Is there a shade flora in the marine plankton? *Journal of Phytoplankton Research*, *4*(2), 391–399. https://doi.org/10.1093/plankt/4.2.391

Stickley, C. E., Pike, J., Leventer, A., Dunbar, R., Domack, E. W., Brachfeld, S., et al. (2005). Deglacial ocean and climate seasonality in laminated diatom sediments, Mac. Robertson Shelf, Antarctica. *Palaeogeography, Palaeoclimatology, Palaeoecology*, *227*(4), 290–310. https://doi.org/10.1016/j.palaeo.2005.05.021

Strub, P. T., Mesías, J. M., Montecino, V., Rutllant, J., & Salinas, S. (1998). Coastal Ocean circulation off Western south America, coastal segment. In A. R. Robinson & K. H. Brink (Eds.), *The Sea*, volume 11. The global coastal ocean, regional studies and synthesis (Vol. 11, pp. 273–313). Wiley.

Suess, E., von Huene, R., & Scientific Party. (1988). *Proceeding of the ocean drilling program.* Initial Reports 112. Ocean Drilling Program.

Tesi, T., Belt, S. T., Gariboldi, K., Muschitiello, F., Smik, L., Finocchiaro, F., et al. (2020). Resolving sea ice dynamics in the North-Western Ross Sea during the last 2.6 ka: From seasonal to millennial timescales. *Quaternary Science Reviews*, *237*, 106299. https://doi.org/10.1016/j.quascirev.2020.106299

Thornburg, T. M., & Kulm, L. D. (1981). Sedimentary basins of the Peru continental margin: Structure, stratigraphy, and cenozoic tectonics from 6°S–16° latitude. In L. D. Kulm, J. Dymond, E. J. Dasch, & D. M. Hussong (Eds.), *Nazca Plate: Crustal formation and andean convergence* (Vol. 154, pp. 393–422). Geological Society of America.

Thunell, R., Pride, C., Tappa, E., & Muller-Karger, F. (1993). Varve formation in the Gulf of California: Insights from time series sediment trap sampling and remote sensing. *Quaternary Science Reviews*, *12*(6), 451–464. https://doi.org/10.1016/s0277-3791(05)80009-5

Wara, M. W., Ravelo, A. C., & Delaney, M. L. (2005). Permanent El Niño-like conditions during the Pliocene Warm Period. *Science*, *309*(5735), 758–761. https://doi.org/10.1126/science.1112596

Wefer, G., Berger, W. H., & Richter, C. (1998). The Angola-benguela upwelling system: Paleoceanography synthesis of shipboard results from LEG 1751. Initial Reports. 175. *Proceeding of the ocean drilling program.* Texas A&M University.

White, S. M., & Ravelo, A. C. (2020a). The benthic B/Ca record at site 806: New constraints on the temperature of the West Pacific warm Pool and the "El Padre" state in the Pliocene. *Paleoceanography and Paleoclimatology*, *35*(10), e2019PA003812. https://doi.org/10.1029/2019pa003812

White, S. M., & Ravelo, A. C. (2020b). Dampened El Niño in the early Pliocene Warm Period. *Geophysical Research Letters*, *47*(4), e2019GL085504. https://doi.org/10.1029/2019gl085504

Zhang, Y. G., Pagani, M., & Liu, Z. (2014a). A 12-million-year temperature history of the tropical Pacific Ocean. *Science*, *344*(6179), 84–87. https://doi.org/10.1126/science.1246172

Zhang, Y. G., Pagani, M., & Liu, Z. (2014b). Response to comment on "A 12-million-year temperature history of the tropical Pacific Ocean". *Science*, *346*(6216), 1467. https://doi.org/10.1126/science.1257930

## Erratum

In the originally published version of this article, author Anna Gioncada's surname was misspelled as "Gionacada." This error has been corrected, and this may be considered the authoritative version of record.